A mix design methodology of blast furnace slag and fly ash-based alkali-activated concrete

Sun, Beibei; Sun, Yubo; Ye, Guang; De Schutter, Geert

A mix design methodology of blast furnace slag and fly ash-based alkali-activated concrete

Beibei Sun [a], Yubo Sun [a], Guang Ye [a,b,**], Geert De Schutter [a,*]

[a] *Ghent University, Department of Structural Engineering and Building Materials, Magnel-Vandepitte Laboratory, Technologiepark-Zwijnaarde 60, 9052, Ghent, Belgium*
[b] *Microlab, Section Materials and Environment, Faculty of Civil Engineering and Geosciences, Delft University of Technology, Stevinweg 1, 2628 CN, Delft, the Netherlands*

A B S T R A C T

Although the application of blast furnace slag and fly ash-based alkali-activated concrete (BFS/FA-AAC) has both economic and environmental benefits, it is limited by the lack of a straightforward mix design method. In this paper, an experiment was conducted to investigate the effect of control factors, including the Na_2O/binder ratio, the SiO_2/Na_2O ratio, the BFS/binder ratio, the water/binder ratio, and the water content on the workability (slump and rheology) of BFS/FA-AAC, and the effect of control factors include the Na_2O/binder ratio, the SiO_2/Na_2O ratio, the BFS/binder ratio, the water/binder ratio, and the curing time on the compressive strength of BFS/FA-AAC. As a result, the influence degree and mechanism of each control factor on the performance of BFS/FA-AAC were quantitively explored and the accuracy of an empirical compressive strength formula was validated. Based on that, a practical mix design method of BFS/FA-AAC was eventually established. It is found that the mixture composition and content of paste can significantly influence the workability of BFS/FA-AAC. The compressive strength of BFS/FA-AAC is determined by control factors when the water content is within 160–195 kg/m^3. The mechanical predictive method of BFS/FA-AAC is proven of high accuracy. The mixture designed by this methodology exhibits satisfied fresh and hardened performance as well as high environmental benefits.

1. Introduction

Alkali-activated concrete (AAC) is a potential replacement for Portland cement concrete (PC concrete) [1–3], which is mainly produced by the alkali activation of silica and alumina-rich materials using alkaline activators. As the most common industrial by-products, blast furnace slag (BFS) and fly ash (FA) have rich silica-alumina sources, which show great utilization value as precursors in AAC. The utilization of them can not only contribute to the ecological cycles (reducing carbon footprint) but also reduce the economic pressure on waste disposal [4,5].

Previous research has shown a good synergy of BFS and FA in AAC, providing both preferable mechanical properties and durability, compared to AAC produced by a single precursor. Besides, BFS/FA-AAC possesses lots of advantages, such as rapid strength gaining, low thermal conductivity, high volume stability, fire resistance, and chemical erosion resistance [6–16]. Since the 1950s, BFS/FA-AAC has received more and

more attention from both academic and industry fields and its application has developed rapidly.

However, compared with PC concrete, the AAC application achievements were accomplished through long exploration. The first and biggest difficulty comes from mix design. Normally, the final BFS/FA-AAC mixture for an industrial application or academic research is determined by proposing a series of empirical mixing proportions and screening out the mixture with the best performance through extensive labour-consuming tests [17–23]. The fault tolerance rate of this method is rather low due to the relatively long curing time of BFS/FA-AAC. Previous research has found that it takes 90 days for the compressive strength of BFS/FA-AAC to reach stable [24–27]. Therefore, at least another 90 days is needed to redesign the mix proportion and redo the tests, which is time-consuming [28,29]. Despite that, the redesign is not guaranteed since the effects of different factors on the properties of BFS/FA-AAC have not been systematically investigated yet. Therefore,

even though BFS/FA-AAC has good application prospects, its widespread utilization is still restricted. Nowadays, the urgent task of popularizing BFS/FA-AAC is to put forward a suitable, practical, and straightforward mix design method.

The effect of certain factors of BFS/FA-AAC on the fresh and hardened properties has been studied to some extent and some guidance regarding the mix design of BFS/FA-AAC was proposed by literature. T. Phoo-ngernkham et al. studied the effect of NaOH concentration (from 5 M to 15 M), alkaline activator solution to fly ash ratio (from 0.45 to 0.60), the coarse aggregate size (average value from 7 mm to 16 mm) on the slump, and 28 d compressive strength of high calcium FA-AAC, and proposed a mix design procedure [30]. M. Talha Junaid et al. investigated the influence of water to solid ratio (from 0.23 to 0.29), alkaline activator to fly ash ratio (from 0.3 to 0.55) on the slump, and 7 d compressive strength of FA-AAC and presented mix design graphs [20]. N. Li et al. studied the effect of water to binder ratio (from 0.4 to 0.5), fly ash to binder ratio (from 0.2 to 0.4), excess paste thickness (from 52 μm to 66 μm), Na_2O to binder ratio (from 4% to 7%), modulus in sodium silicate (from 0 to 2) on the slump, and 28 d compressive strength of BFS/FA-AAC and proposed mix design guidance [31]. Ali Rafeet et al. studied the effect of paste volume (from 0.3 to 0.33), BFS content (from 0 to 0.7), and water to solid ratio (from 0.35 to 0.48) on the slump and 28 d compressive strength of BFS/FA-AAC and put forward several guidelines for the mix design [19].

These researches deepened the understanding and provided preliminary suggestions for the mix design of BFS/FA-AAC. However, the proposed guidance could be incomparable, due to the restricted research mix proportion range and curing time, overlapping of some important influencing factors, and omission of differences in attributes of the raw materials with different resources (eg: concentration of NaOH, the molar ratio of Na_2SiO_3, the reactivity of BFS and FA). Besides, the relatively broad suggestions might have limited guidance on the specific calculation of mix proportion. Moreover, despite the independent research, it is also unrealistic to generalize mix design methods of BFS/FA-AAC from the accumulated research literature due to the non-uniformed mix design parameters of different literature. In general, the unavailability of mix design methods of BFS/FA-AAM nowadays is primarily attributed to the instability of raw material characteristics, the complexity of multiple raw material combinations, as well as the unreproducible and incomparable current research results due to the lack of unified design factors.

A critical awareness for developing a practical mix design method for BFS/FA-AAC is to have a systematic investigation process based on representative design factors and range. This requires solving the correlative problems one by one progressively under the unified research system. Previous research has summarized the raw materials requirements for stable performance of BFS/FA-AAC and proposed control factors of BFS/FA-AAC from the reaction mechanism aspect [32]. By investigating the influence of the control factors on the fresh and hardened properties of blast furnace slag and fly ash-based-alkali activated paste (BFS/FA-AAP), the workability and mechanical properties evaluation methods and mix design methods of BFS/FA-AAP were proposed, which lays a stable foundation for further exploration of the combined effect of BFS/FA-AAP and aggregates in BFS/FA-AAC [29]. Based on that, the effect of a larger number of components and their characteristics (BFS, FA, NaOH, Na_2SiO_3, water, aggregates, concentration of NaOH, the molar ratio of Na_2SiO_3, the reactivity of BFS and FA) incorporated in the reaction systems of BFS/FA-AAC could be simplified into two subsets: BFS/FA-AAP and aggregates, which simultaneously influence the fundamental performance (workability and mechanical properties) of BFS/FA-AAC. With this research concept, the combined influence of BFS/FA-AAP and aggregate on the performance of BFS/FA-AAC is the key to the current research.

The effect of BFS/FA-AAP and aggregate on the properties of BFS/FA-AAC has been proceeding studied and reported in literature. Hung et al. found that both slump and mechanical properties of BFS/FA-AAC increase with the AAP/aggregate ratio of 0.4–0.7, and decrease with the

fine aggregate/coarse aggregate ratio of 0–0.8 [33]. S. Haruna et al. reported that the AAP/aggregate ratio of BFS-AAC from 0.35 to 0.57 is proportional to its slump, while inversely proportional to its compressive strength [34]. A. Rafeet et al. found that the influence of the paste volume from 30% to 33% on the compressive strength of BFS/FA-AAC is negligible. But the slump of BFS/FA-AAC improves significantly with higher paste volume [19]. Vinai et al. noted that the slump and compressive strength of BFS/FA-AAC increase with higher paste volume (from 0.29 to 0.43) [35].

From the above research, it can be concluded that the AAP/aggregate ratio could improve the slump. However, there is no unified understanding of its influence of it on compressive strength. The possible reason could be derived from the PC concrete design concept: too high paste content could lead to segregation (an uneven aggregate distribution), and shrinkage problems, while too low paste content could lead to insufficient aggregate bonding and the introduction of harmful pores in the microstructure. Given that, the paste content boundary of BFS/FA-AAC is of great importance for the mix design of BFS/FA-AAC, though it has not been studied yet.

Except that the paste content design of BFS/FA-AAC is restricted by the lack of a comprehensive study, there is not yet quantitive research on the effect of all control factors on the fundamental properties (slump and compressive strength) of BFS/FA-AAC, which makes it difficult to accurately adjust the mix proportion of BFS/FA-AAC after the trial test. Given these deficiencies, a systematic exploration of the effect of control factors on the fundamental properties of BFS/FA-AAC is critical.

In this paper, an experiment is conducted to investigate the workability and compressive strength of BFS/FA-AAC with various mix proportions. The research objectives are: 1) to clarify the effect of the control factor (the Na_2O/b ratio, the SiO_2/Na_2O ratio, the w/b ratio, the BFS/b ratio, water content) on the slump and rheology of BFS/FA-AAC; 2) to explore the paste content boundary of BFS/FA-AAC and to understand the influence of control factors (the Na_2O/b ratio, the SiO_2/Na_2O ratio, the w/b ratio, the BFS/b ratio, and curing time) on the compressive strength of BFS/FA-AAC; 3) to establish a practical mix design method for BFS/FA-AAC serving in ordinary environments (no risk of corrosion or attack according to EN 206) and to verify it by a case study.

2. Materials and methods

2.1. Materials

The precursors used in this research were BFS and class F FA from ECOCEM (Moerdijk, The Netherlands) and VLIEGASUNIE (Amsterdam, The Netherlands), respectively. The quantitative X-ray diffraction and X-ray fluorescence analysis techniques show that the vitreous phase contents of BFS and FA are 100% and 68%, respectively. And the specific gravities of BFS and FA are 2890 kg/m^3 and 2300 kg/m^3, respectively. The chemical composition of BFS and FA are shown in Table 1 and the particle distributions of BFS and FA are presented in Fig. 1.

Sodium hydroxide pearls and sodium silicate solution from BRENNTAG (Deerlijk, Belgium), were used with tap water to prepare the alkali activator. The concentration of sodium hydroxide is 99%. The sodium silicate solution includes 27.5 wt% SiO_2, 8.25 wt% Na_2O, and 64.25 wt% H_2O. The densities of sodium hydroxide and sodium silicate are 2130 kg/m^3 and 1350 kg/m^3, respectively.

The aggregates used in this study were medium size (aggregate 1: 8–16 mm), small size (aggregate 2: 2–8 mm) coarse aggregate, and 0–4 mm river sand. The saturated and surface-dried particle densities are 2619 kg/m^3, 2589 kg/m^3, and 2644 kg/m^3, respectively. The loose bulk densities are 1548 kg/m^3, 1559 kg/m^3, and 1652 kg/m^3, respectively. The fineness modulus of sand is 2.92. Specifically, the particle distributions of coarse aggregates and sand are presented in Fig. 1. The aggregate grading used in this research is A16, which is an aggregate size distribution suggested in the European standard: EN 206 (see

Table 1
Chemical composition of BFS and FA measured by XRF (wt%).

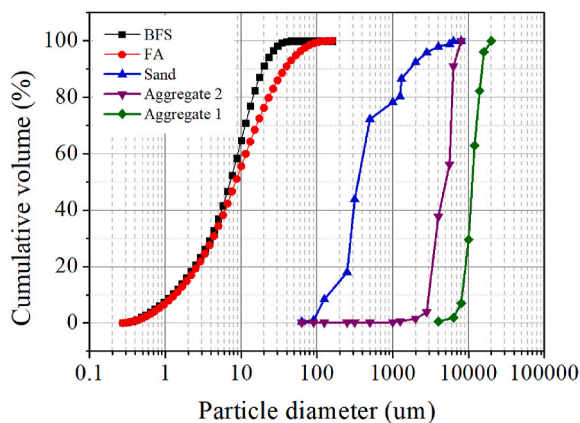| Element	BFS	FA
SiO_2	31.1	56.7
CaO	40.9	3.74
Al_2O_3	13.7	24
MgO	9.16	1.75
Fe_2O_3	0.401	2.3
MnO	0.31	0.0579
CuO	0.0054	0.0149
Rb	0.0032	0.0109
SO_3	2.31	1.04
ZrO_2	0.119	0.103
SrO	0.0741	0.129
Ti_2O	1.26	1.16
As	0.0006	0.0071
ZnO	0.003	0.0238
K_2O	0.685	–
Na_2O	–	1.94
Other components	0	7.0234

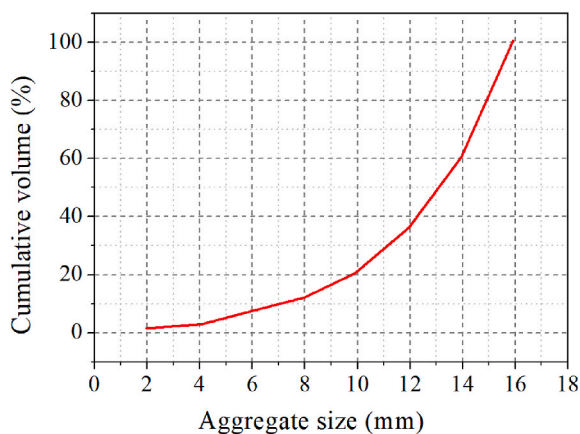**Fig. 1.** Particle size distributions of raw materials.

Fig. 2. Aggregate grading.

Fig. 2).

2.2. Mixture proportions and mixing protocols

To understand the effects of different control factors on the performance of BFS/FA-AAC, in total 27 groups of the sample were prepared. The mix proportions of BFS/FA-AAC are presented in Table 2. The final activators were prepared by pre-dissolving the sodium hydroxide pearls in sodium silicate solution and tap water according to the mix

Table 2
Mixture proportion.

Group	Na_2O/b (%)	SiO_2/Na_2O	w/b	BFS/b	Water content (kg/m^3)	Aggregate
1	4	0	0.4	1	160	A16
2	4	0	0.4	1	180	
3	4	0	0.4	1	195	
4	4	0.5	0.5	1	160	
5	4	0.5	0.5	1	180	
6	4	0.5	0.5	1	195	
7	4	0.5	0.4	1	160	
8	4	0.5	0.4	1	180	
9	4	0.5	0.4	1	195	
10	4	0.25	0.4	1	160	
11	4	0.25	0.4	1	180	
12	4	0.25	0.4	1	195	
13	2	0.5	0.4	1	160	
14	2	0.5	0.4	1	180	
15	2	0.5	0.4	1	195	
16	4	0	0.4	0.5	160	
17	4	0	0.4	0.5	180	
18	4	0	0.4	0.5	195	
19	4	0.5	0.4	0.5	160	
20	4	0.5	0.4	0.5	180	
21	4	0.5	0.4	0.5	195	
22	4	0	0.4	0.75	160	
23	4	0	0.4	0.75	180	
24	4	0	0.4	0.75	195	
25	4	0.5	0.4	0.75	160	
26	4	0.5	0.4	0.75	180	
27	4	0.5	0.4	0.75	195	

proportion a day before casting. The BFS/FA-AAC mixtures were prepared in a concrete mixer by the following procedure: 1) All solid materials were premixed for 1 min; 2) The alkali-activated solution was then added and mixed for 1 min; 3) The layer of mixture sticking to the mixing arm, the walls, and bottom of the mixing bowl was scraped and recollected during 1 min of rest. 4) The mixture continued to be mixed for another 2 min.

After proper mixing, each mixture was cast in 3 cubic molds (150 × 150 × 150 mm^3) and immediately covered with a plastic layer to avoid moisture loss. All specimens were then stored in a room with a temperature of 20 °C and relative humidity higher than 90%. The samples were demolded after 1 day, sealed with 2 layers of plastic wrap, and then cured at ambient curing conditions (20 ± 2 °C, 60% relative humidity) till the compressive strength testing day (1 d, 7 d, 28 d, 90 d).

2.3. Testing program

The slump and rheology of BFS/FA-AAC were tested immediately after mixing. The number of repetitions in slump and rheology tests is 3 and 2, respectively. The slump value was obtained according to BS EN 12350–2:2009. The fresh BFS/FA-AAC was poured into a cone-shaped apparatus and then compacted. The slump value was obtained by measuring the distance dropped by the mixture, after lifting the slump cone apparatus upwards. The rheology of BFS/FA-AAC is characterized by static yield stress, dynamic yield stress, and plastic viscosity, which were determined by the shear history-dependent. The measurement was conducted by a four-bladed propeller ICAR rheometer that consists of a vane (height and diameter of 130 mm), a container (diameter of 286 mm, volume of 20 L), and a calculation software that calculates the Bingham model parameters (dynamic yield stress and plastic viscosity) based on Reiner-Riwlin equation [36]. The revolution of the stress growth test is 0.025 rev/s, and the shear protocol is shown in Fig. 3.

The compressive strength of BFS/FA-AAC was measured on the testing day according to BS EN 12390–3:2009. In this research, the compressive strength value of BFS/FA-AAC was recorded as an average of 3 samples and the standard deviation was calculated.
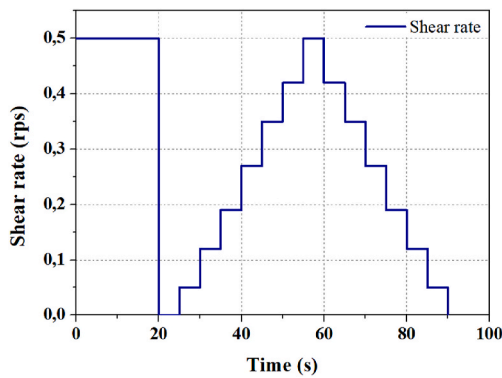
Fig. 3. Shear protocol.

3. Results and discussions

### 3.1. Effect of control factors on the workability of BFS/FA-AAC

It is known that the workability of Portland cement concrete (PC concrete) primarily depends on the maximum aggregate size, aggregate grading, and water content. From the same physical point of view, the performance of BFS/AF-AAC could achieve the best result when the maximum aggregate size meets the structural requirements and the aggregate grading is continuous, as suggested in EN 206.

Nevertheless, a notable difference between the PC concrete mix design and BFS/FA-AAC mix design regarding slump should be emphasized in the paste design. According to American standards and European standards (ACI 211.1–91 and EN 206), the slump design of a PC concrete is directly associated with the water content and maximum aggregate size. The latter is usually designed by the dimension of a construction structure. It illustrates that the paste/aggregate ratio plays a dominant role in the mix design of PC concrete regarding slump. In contrast, the influence of the w/b ratio and the chemical composition of cement are ignored. More specifically, for putting forward a practical mix design method of PC concrete regarding slump, a simplified correlation between slump, water content, and maximum aggregate size was derived, with an assumption that changes in the mix proportion of the cement paste will not affect the slump PC concrete [37]. However, this assumption is no longer practical in the BFS/FA-AAC design, since the performance of BFS/FA-AAP (which is determined by the control factors) is observed to have considerable influence on the slump of BFS/FA-AAC. It will be discussed subsequently.

The effect of the Na_2O/b ratio on the slump of BFS/FA-AAC is presented in Fig. 4(a). According to the experimental results, the slump of BFS/FA-AAC tends to increase with a higher Na_2O/b ratio under low alkali concentration circumstances. Specifically, with every 1% increase in the Na_2O/b ratio, the slump value increases by around 62 mm. This is mainly because of the increase in the total alkali solution volume (the sum of Na_2O, SiO_2, and water). The increase in Na_2O content could lead to an increase in SiO_2 content, which eventually rise the total alkali solution volume in the paste. Therefore, precursor particles in the paste
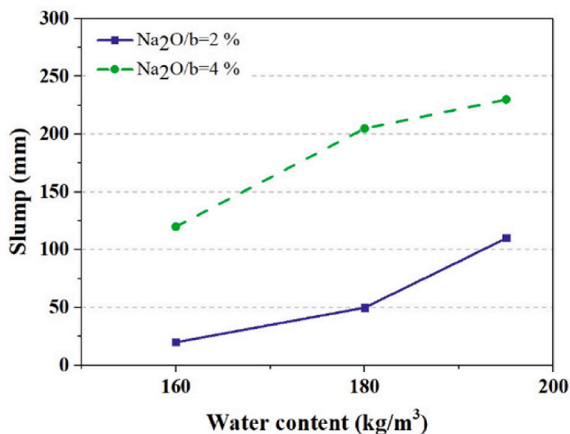
(a) Slump
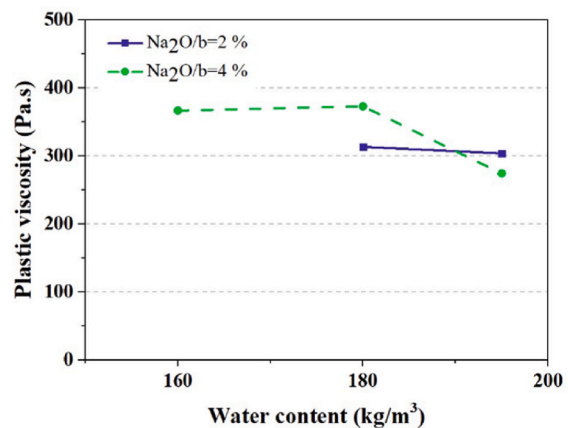
(b) Plastic viscosity
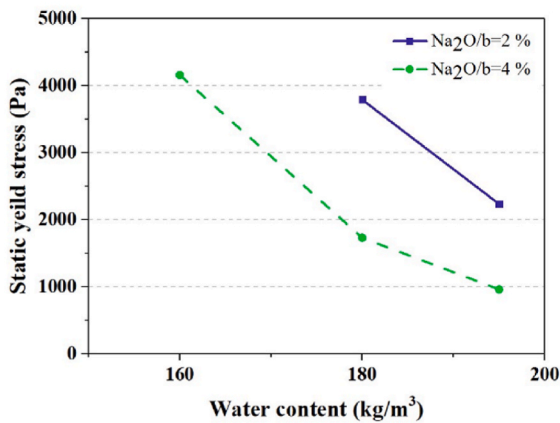
(c) Static yield stress

(d) Dynamic yield stress

Fig. 4. Effect of the Na_2O/b ratio on the workability of BFS/FA-AAC.

tend to be more dispersed. The observation suggests that the influence of the Na$_2$O/b ratio on the flowability of AAP could be reflected in the slump of concrete.

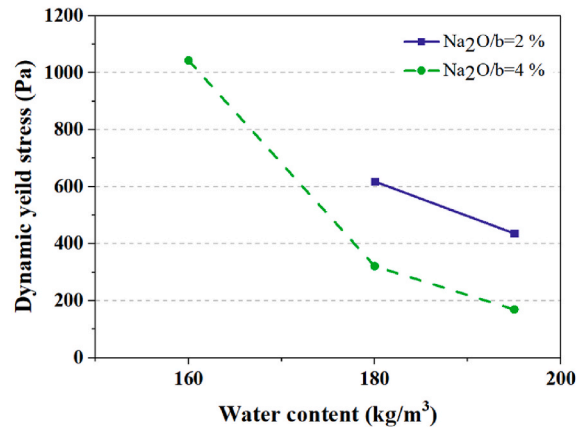The rheology results of BFS/FA-AAC provides further interpretation for the slump decrease with a higher Na$_2$O/b ratio. As illustrated in Fig. 4(b–d), the BFS/FA-AAC mixture with every 1% increase of Na$_2$O/b ratio is associated with approximately 56% (1665 Pa) lower static yield stress and 55% (282 Pa) lower dynamic yield stress, despite the plastic viscosity does not change drastically. It indicates that the stress required for a BFS/FA-AAC mixture to initiate and maintain flowing is relatively lower when BFS/FA-AAC has a higher Na$_2$O/b ratio. This is could be attributed to the rise of the solution to binder ratio caused by the addition of Na$_2$O and SiO$_2$ components. The more dispersed precursor particles could reduce the friction thus leading to better workability.

The slump value of BFS/FA-AAC remarkably rises with the increase of the SiO$_2$/Na$_2$O ratio. As indicated in Fig. 5(a), the slump value increases by approximately 24 mm with every 0.1 increase in the SiO$_2$/Na$_2$O ratio. The proportional relationship was observed in previous research as well [38–41].

Besides, the rheology results demonstrated that the effect of the SiO$_2$/Na$_2$O ratio on the slump of BFS/FA-AAC can not be ignored. As presented in Fig. 5(b–d), with every 0.1 increase in the SiO$_2$/Na$_2$O ratio, the plastic viscosity of the BFS/FA-AAC mixture increased by around 10% (38 Pa.s), the static yield stress decreased by 4% (92 Pa), and the dynamic yield stress decreased by 8% (43 Pa) when the water content is 195 kg/m^3. It suggests that BFS/FA-AAC mixture with a higher SiO$_2$/Na$_2$O ratio is easier to initiate and maintain flowing compared with that

activated by solely NaOH. However, the velocity of the mixture deformation under shear stress could be reduced when increasing the Si concentration in the alkali activator. On the one hand, increasing the viscosity of the alkali-activated solution creates a thicker coating on the surface of precursor particles, which further reduces the internal friction between particles [29,42]. On the other hand, the resistance offered by the BFS/FA-AAC mixture to flow freely could be higher due to the growth of the internal friction between the precursor particle and solution and between solution and solution. The opposite effect was observed for BFS/FA-AAC with a water content of 160 kg/m^3. The plastic viscosity, static yield stress, and dynamic yield stress of BFS/FA-AAC with a SiO$_2$/Na$_2$O ratio of 0.25 are slightly lower than those of BFS/FA-AAC with a SiO2/Na2O ratio of 0.5. Further studies are recommended to explore the possible interaction effect between the SiO$_2$/Na$_2$O ratio and water content on the rheology of BFS/FA-AAC.

The increase of the BFS/b ratio significantly impacts the slump of BFS/FA-AAC (see Fig. 6(a)). With every 0.1 increase in the BFS/b ratio, the slump value of BFS/FA-AAC decreases by about 8–20 mm. It is worth mentioning that the effect of the BFS/b ratio on the slump decline rate of BFS/FA-AAC should be highly regarded. According to previous research, the slump of BFS/FA-AAC might drop rapidly over time when a high BFS content is adopted in the mixture [29].

A similar phenomenon was observed in the rheology results. As illustrated in Fig. 6(b–d), a 0.5 increase of the BFS/b ratio in the BFS/FA-AAC mixture remarkably increases the plastic viscosity by about 67% (226 Pa.s) and increases the static yield stress by 77% (1762 Pa). This could be attributed to the particle shape difference between BFS and FA.
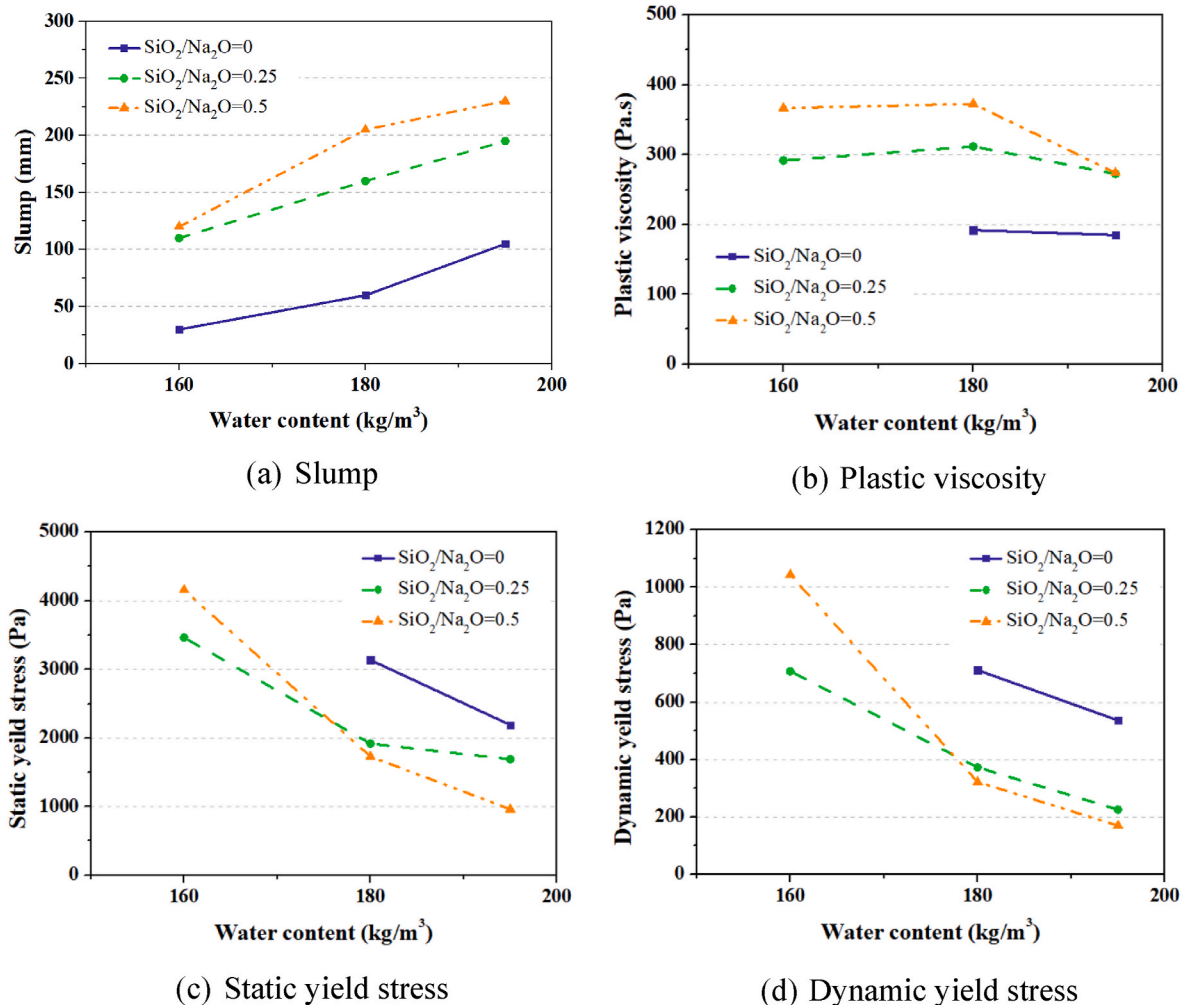

(a) Slump

(b) Plastic viscosity

(c) Static yield stress

(d) Dynamic yield stress

Fig. 5. Effect of the SiO$_2$/Na$_2$O ratio on the workability of BFS/FA-AAC.

(a) Slump

(b) Plastic viscosity

(c) Static yield stress
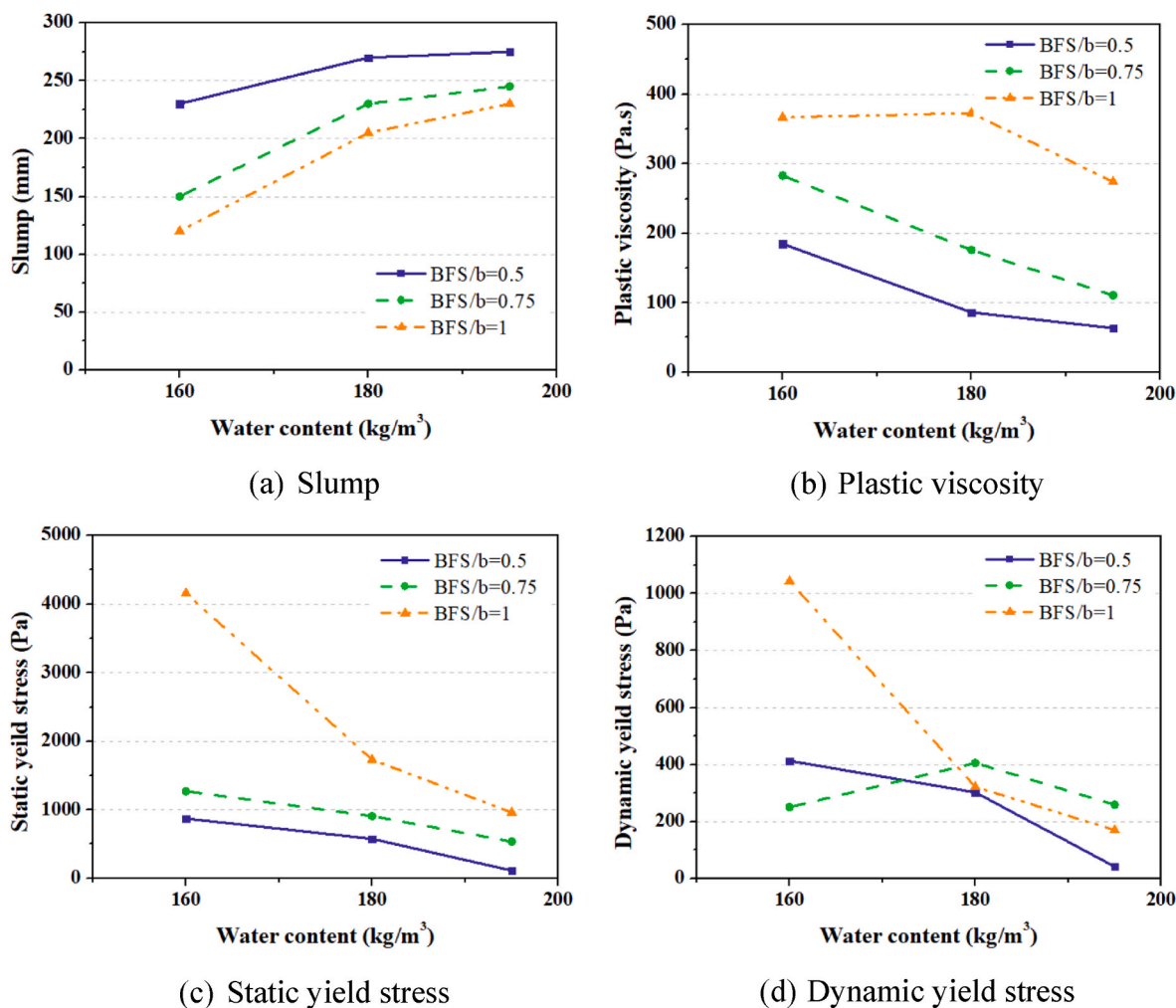
(d) Dynamic yield stress

Fig. 6. Effect of the BFS/b ratio on the workability of BFS/FA-AAC.

Compared with spherical FA particles, BFS particles have an irregular shape which both increases the particle surface area and reduces the "ball-bearing effect". Accordingly, the BFS/FA/AAC mixture with a higher BFS/b ratio has less tendency to initiate flowing and higher resistance during flowing.

The effect of the w/b ratio on the slump of BFS/FA-AAC is demonstrated in Fig. 7(a). It is observed that the slump value of BFS/FA-AAC increases by around 6 mm with every 0.01 increase of the w/b ratio. Previous research suggests that the w/b ratio might have little influence on the slump of BFS/FA-AAC decrease over time [29].

The increase of the w/b ratio in the BFS/FA-AAC mixture also significantly decreases the plastic viscosity and reduces both static yield stress and dynamic yield stress. It is reasonable since a higher w/b ratio increases the distance between the precursor particles, thus reducing the friction between them.

As highly paste-coated aggregates reduce internal friction thus resulting in a higher slump of BFS/FA-AAC. The slump value of BFS/FA-AAC significantly increased by around 27 mm with every 10 kg/m³ of water content. Besides, reductions in plastic viscosity, static yield stress, as well as dynamic yield stress were observed for BFS/FA-AAC mixture at higher water content, regardless of the mix proportion variation in the paste.

3.2. Effect of control factors on the compressive strength of BFS/FA-AAC

Generally, the compressive strength of a material is controlled by porosity. Similarly, the compressive strength of PC concrete is determined by the porosity of each constituent phase, which includes the paste porosity, aggregate porosity, and interfacial transition zone porosity [43]. According to American and European standards (ACI 211.1–91 and EN 206), the compressive strength is directly associated with the paste porosity, which is controlled by cement type and w/c ratio, while the effect of the aggregates and transition zone is ignored. This simplified correlation is derived under the understanding that the aggregate porosity is normally much lower than the other phases. And the effect of interfacial transition zone porosity is neglectable though it could be the "weak link".

This design assumption is even more practical in BFS/FA-AAC when the strength of the selected aggregate is higher than that of the paste because the interfacial transition zone in BFS/FA-AAC is no longer the weakest region [44]. Compared with the transition zone of PC concrete, the aggregate-paste interface of both BFS-AAC and FA-AAC has been detected to be denser, more cohesive, and uniform [45,46]. On the one hand, the soluble Si in the alkali activator increases the bonding between aggregate and paste [47]. On the other hand, reaction products with a lower Ca/Si ratio are generated instead of the expansive (Al-free) gels [48–50], which results in fewer cracks in the transition zone.

This inference is further verified by the experimental results in this research, as presented in Fig. 8. A Kolmogorov-Smirnov test was conducted to evaluate the statistical distribution of the experimental data in this paper. The significant factor of data regarding slump and compressive strength is 0.265 and 0.384, respectively, both higher than 0.05. This show that both slump and compressive strength value in this research do not fit a normal distribution. Therefore, a Wilcoxon signed-
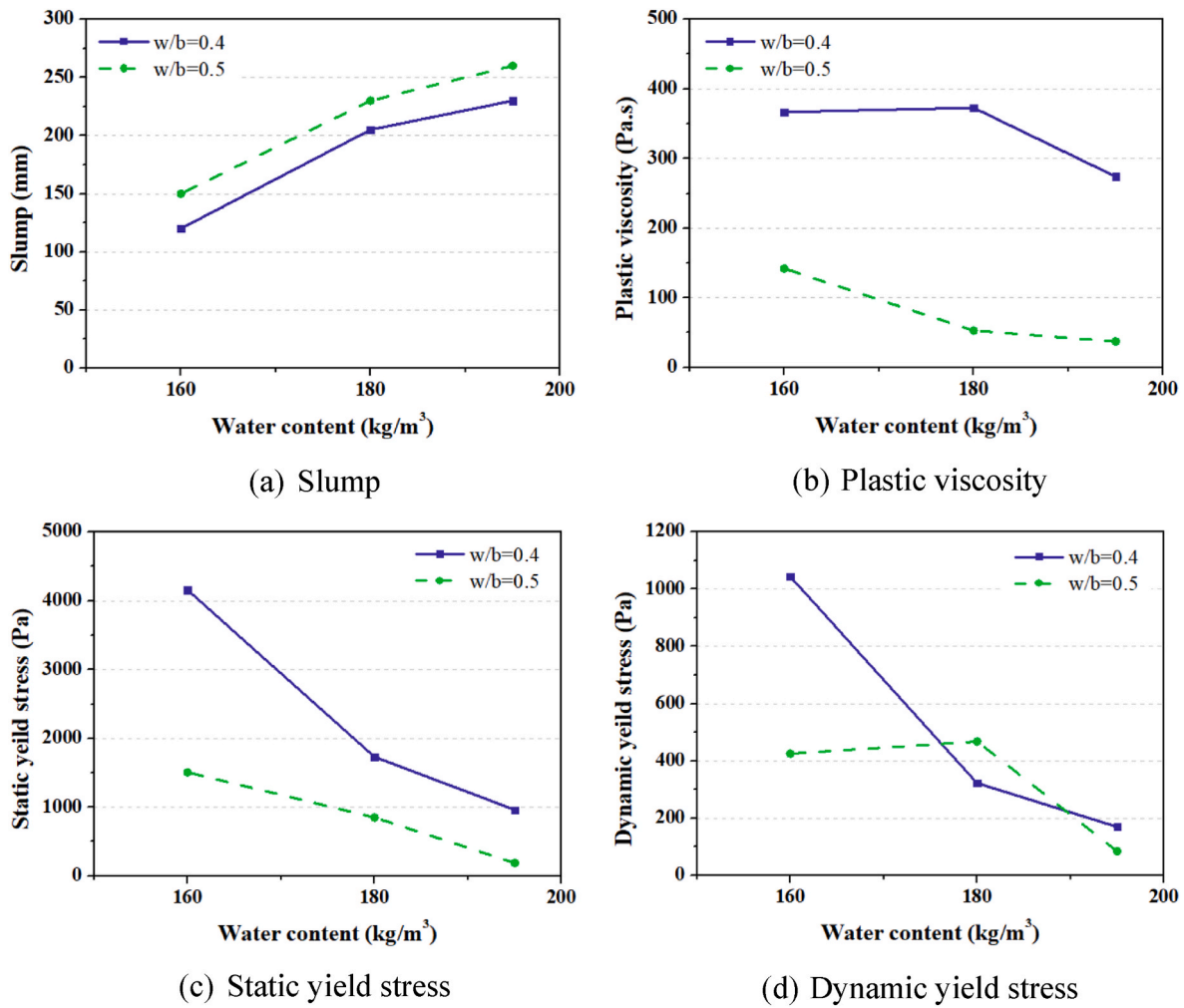
(a) Slump

(b) Plastic viscosity

(c) Static yield stress

(d) Dynamic yield stress

Fig. 7. Effect of the w/b ratio on the workability of BFS/FA-AAC.

rank test is used instead of a parametric statistical test. The Wilcoxon signed-rank test is a non-parametric statistical hypothesis test used either to test the location of a set of samples or to compare the locations of two populations using a set of matched samples. It was carried out by SPSS to quantitatively evaluate the accuracy of the predictive formula (PF) [29] of BFS/FA-AAP (see Eq. (1)) on the prediction of the compressive strength of BFS/FA-AAC. The PF is applicable for evaluating the compressive strength of BFA/FA-AAP when the Na2O/b ratio is between 0 % and 10%, the SiO$_2$/Na$_2$O ratio is between 0 and 2, the w/b ratio is between 0.3 and 0.5, the BFS/b ratio is between 0 and 1, and sealed curing at ambient temperature. The prediction interval of the compressive strength is 95%.

$$fc(X_1, X_2, X_3, X_4, X_5) = (-1.33 + 12.3X_1 + 42.68X_2 - 1.04 \times_1^2 + 2.37 \times 1 \times_2 - 17.05 \times_2^2) \cdot (-1.37X_3 + 1.04X_4 + 1) \cdot 0.2\ln(X_5 + 11.31) \quad (1)$$

In which: X_1 is the Na$_2$O/b ratio (%); X_2 is the SiO$_2$/Na$_2$O ratio; X_3 is the w/b ratio; X_4 is the BFS/b ratio; X_5 is the curing time (d); fc(X_1, X_2, X_3, X_4, X_5) is the compressive strength of BFS/FA-AAP that is sealed and cured at ambient temperature (MPa)

The results show that the experimental compressive strength of BFS/FA-AAC is highly close to the PF-predicted compressive strength. According to the results of the Wilcoxon signed-rank test of the compressive strength over 7d, the median of the test value, and the PF predicted value is 39 MPa, and 38 MPa, respectively. The differences between them were obtained by subtracting the test value from the predicted value. The median of the difference between the test value and the PF

predicted value is −0.78 MPa. The P-value of the test value and PF predicted value is 0.77. The prediction interval of the compressive strength is 95%. It indicates that the difference between the two groups is statistically insignificant. However, regarding the 1 d compressive strength, the median of the test value, and the PF predicted value are 13 MPa, and 27 MPa, respectively. The median of the difference between the test value and the PF predicted value is 13.02 MPa. The P-value of the test value and PF predicted value is 0. The prediction interval of the compressive strength is 95%. It indicates that there are statistically significant differences between the two groups. This shows that the 1 d compressive strength of BFS/FA-AAC is technically and theoretically unpredictable, which could be attributed to the relatively long setting time of BFS/FA-AAP. Previous studies have shown that the BFS/FA-AAP with a low BFS/b ratio might require more than 3 d (less than 7 d) for the strength to start developing [29]. In conclusion, PF is proven with high accuracy in predicting the compressive strength of BFS/FA-AAC after 7 d. Most importantly, it implies that the compressive strength of BFS/FA-AAC is primarily determined by the performance of the BFS/FA-AAP.

Moreover, it can be further inferred that the control factors of BFS/FA-AAP directly determine the compressive strength of BFS/FA-AAC when the water content is within the research range of this study, as presented in Fig. 8. Within 160–190 kg/m^3, the effect of water content on the compressive strength of BFS/FA-AAC is negligible. The stable performance of BFS/FA-AAP suggests that the possible segregation, shrinkage, insufficient aggregate bonding, and harmful pores introduction problems in BFS/FA-AAC are negligible with reasonable paste
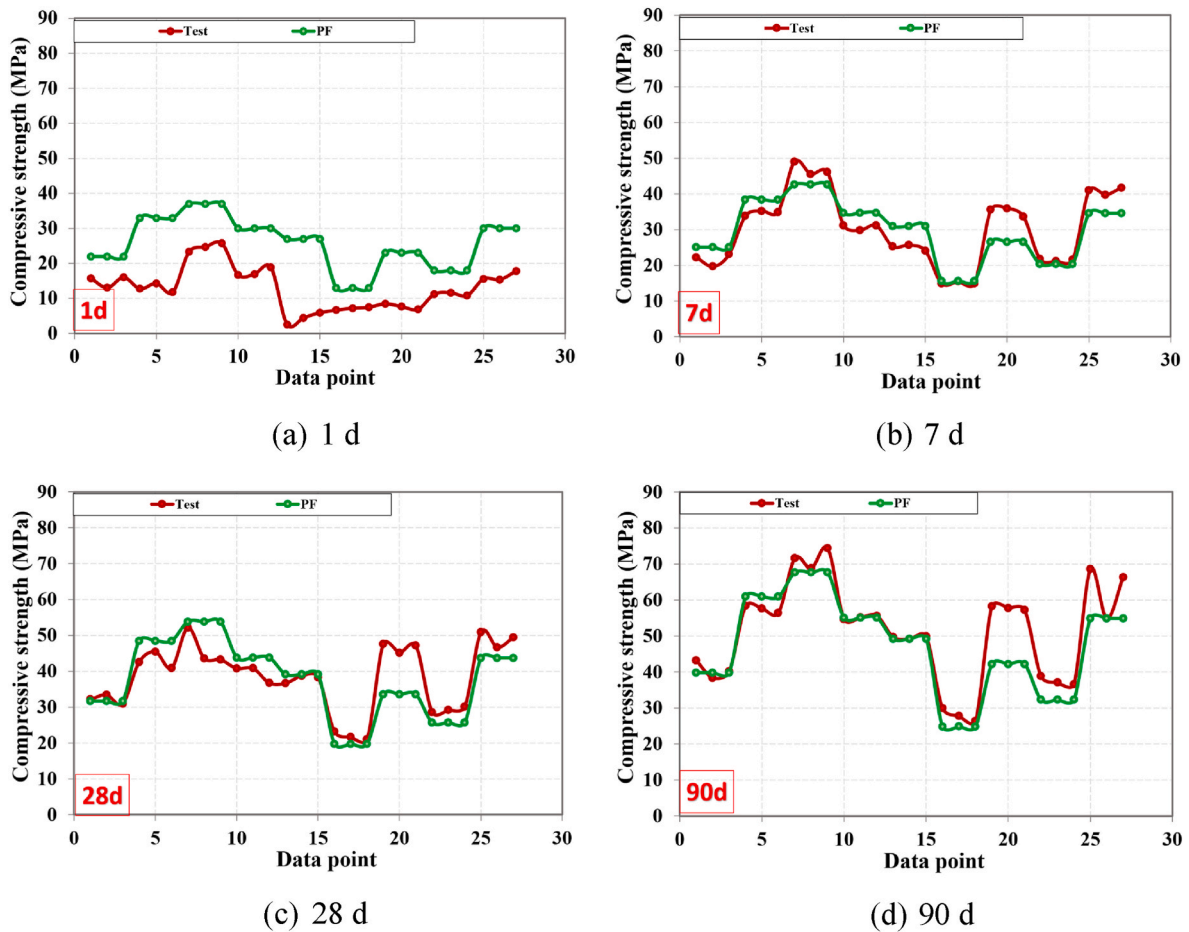
Fig. 8. Comparison between test value and predictive value of BFS/FA-AAC.

content. Under this circumstance, the control factors contribute to the compressive strength of BFS/FA-AAC with different degrees and influence mechanisms, which will be discussed subsequently.

The effect of the control factors on the compressive strength of BFS/FA-AAC is shown in Fig. 9. When the Na_2O/b ratio is from 2% to 4%, the compressive strength of BFS/FA-AAC ($SiO_2/Na_2O = 0.5$, w/b = 0.4, BFS/b = 1, curing time = 90 d) increases by approximately 9 MPa with every 1% increase in the Na_2O/b ratio. This is mainly because the alkali content determines the dissolution rate. Due to the decomposition effect of OH^-, the higher the Na_2O/b ratio, the more ions could be dissolved in the solution, which facilitates further polymerization [42,51,52]. The higher amount of released monomers thus has a higher tendency to be

connected, which accelerates the coagulation period. It is worth noting that the compressive strength of BFS/FA-AAC might decrease with the Na_2O/b ratio when it surpasses 6% [29]. At higher alkali environment, the participation of the $Ca(OH)_2$ layer on the BFS particle surface and the Al–Si gel on the FA particle surface could hinder further reaction of precursors thus reducing the compressive strength of BFS/FA-AAC [53, 54].

The compressive strength of BFS/FA-AAC ($Na_2O/b = 4\%$, w/b = 0.4, BFS/b = 1, curing time = 90 d) increases by 6 MPa with every 0.1 increase of the SiO_2/Na_2O ratio when the SiO_2/Na_2O ratio is within 0–0.5. The introduction of SiO_2 in activators significantly improved the strength because the structure-forming element (Si) in the solution could
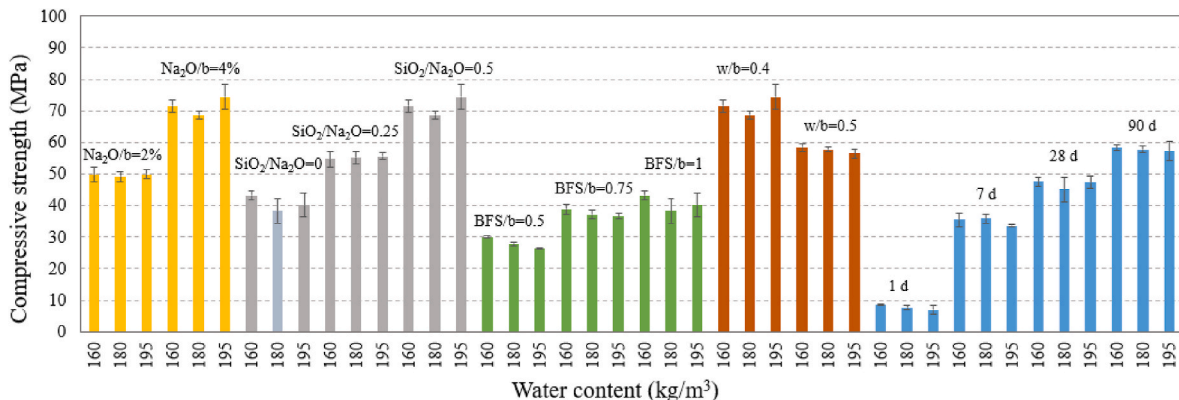

Fig. 9. Effect of the control factors on the compressive strength of BFS/FA-AAC.

act as nuclei sites, which promotes the strength development from two aspects: 1) The dissolution is accelerated since the condensation on the nuclei sites keeps the undersaturation degree of reaction ions (except Si) at a high level. 2) A homogenous and denser microstructure is simultaneously produced because the reaction products could form not only on the surface of precursor particles but also in the solution. It is worth noting that the compressive strength development of BFS/FA-AAC could be reduced with a higher SiO_2/Na_2O ratio, because the precipitation of excess SiO_2 species could hinder the zeolite crystalization and polymerization in the subsequent reaction process [29].

It is found that the compressive strength of BFS/FA-AAC ($Na_2O/b = 4\%$, $SiO_2/Na_2O = 0$, $w/b = 0.4$, curing time = 90 d) substantially increased with the BFS/b ratio. This is due to the different chemical compositions of BFS and FA. The increase in BFS content (higher Ca/Si and Si/Al ratios) could lead to a higher dissolution rate of the reaction system because Ca–O–Si bonds are weaker than Al–O–Si bonds [42]. Eventually, it leads to the formation of a lower polymerization degree and higher cross-linking chain reaction product (more CASH gel and less NASH gel). Because CASH gel has a higher space-filling ability than NASH gel [55–57], a more homogenous and compact structure is produced.

The compressive strength of BFS/FA-AAC drops with the w/b ratio. According to the linear fitting results, the compressive strength of BFS/FA-AAC ($Na_2O/b = 4\%$, $SiO_2/Na_2O = 0.5$, $BFS/b = 1$, curing time = 90 d) slightly decreases by about 1.4 MPa with every 0.01 increase of the w/b ratio. It indicates that the water has less impact on the compressive strength of BFS/FA-AAC, compared with other control factors. It is consistent with previous research demonstrating that the effect of water on the strength of BFS/FA-AAP is much smaller than its effect on the strength of PC concrete [29]. This is because the formation of reaction products in BFS/FA-AAP requires nearly no water[107, 169-171]. Although water helps as an alkali carrier in the reaction process, its existence could reduce the density of the microstructure due to the increasing harmful pores. Therefore, BFS/FA-AAC with less water is associated with higher density and a slightly higher compressive strength [29,58,59].

A higher compressive strength of BFS/FA-AAC ($Na_2O/b = 4\%$, $SiO_2/Na_2O = 0.5$, $BFS/b = 0.5$, $w/b = 0.4$) is associated with longer curing time since it provides more time for the reaction. It is worth noting that compressive strength development with curing time could show a different trend when the mixture proportion of BFS/FA-AAC changes. In general, the higher the BFS, and Na_2O content, the earlier the compressive strength could develop [29].

3.3. A mix design method of BFS/FA-AAC

3.3.1. Mix design principle

From the above results, a mix design method could be eventually established. It is known that the main mix design objective for a construction material serving in ordinary environments is to strike a balance between cost, fresh properties, and hardened properties (compressive strength is considered an indicator of durability) [37]. Besides that, a practical mix design method of BFS/FA-AAC should meet the following principles:

1) A straightforward mathematical model should be proposed, so as to calculate the mix proportion of BFS/FA-AAC more conveniently.
2) All mix design assumptions should be consistent with the realistic material characteristics of BFS/FA-AAC.
3) A robust correspondence should exist between the designed mix proportions and the designed ultimate performance, regardless of different operational origins.
4) The concept of cost management should be reflected in the mix design method for efficient application in engineering.
5) The mix design method of BFS/FA-AAC should respect the conventional design habits of PC concrete (build on the current classification of raw materials, performance indicators, etc, and closely related to the PC concrete design standard), considering that BFS/FA-AAC is a potential substitute for PC concrete.

3.3.2. Mix design procedure

Based on the mix design principles, a mix design procedure is proposed, as demonstrated in Fig. 10. With a simplified mix design method of BFS/FA-AAP [29], the understanding of the reactivity requirement of raw materials [32], and the awareness of how different control factors influence the workability and compressive strength of BFS/FA-AAC, a mix design method of BFS/FA-AAC is eventually established. Following the mix design procedure, a mix proportion satisfying the expected performance could be derived step by step, which will be further discussed.

3.3.2.1. BFS/FA-AAP design.
The first step for designing a BFS/FA-AAC mix is to set up the required mechanical properties, i.e., compressive strength, and fresh properties like setting time, and workability of BFS/FA-AAC based on the construction type. Afterwards, the mixture proportion of BFS/FA-AAP could be designed according to Table 3, based on the principle of satisfying these required early properties, following the instructions of the previous study [29]. Considering the mix design of BFS/FA-AAP is a balance between economic, strength, setting time, and workability, several rules should be emphasized during the selection: 1) A lower Na_2O/b ratio and a higher corporation of the readily available precursor is suggested for the economical benefit; 2) A higher SiO_2/Na_2O ratio, and/or a higher w/b ratio, and/or a lower BFS/b ratio are suggested for obtaining high flowability; 3) A higher BFS/b ratio and/or a higher Na_2O/b ratio is suggested for the AAP that requires rapid coagulation, and vice versa.

3.3.2.2. Raw materials selection.
Except for a proper mix design, the high quality of the raw materials is also of great importance for achieving the performance shown in Table 3, which means the polymerization process should not be affected by the low reactivity of precursors. Unlike cement, the physical and chemical characteristics of BFS and FA vary from origin. The different glassy phase content, particle size, and chemical composition would inevitably influence the reactivity of the precursors. For selecting qualified precursors in the application of BFS/FA-AAC, the physical and chemical requirements of BFS and FA are presented in Table 4. Besides, it is worth mentioning that the aggregate strength should be larger than the BFS/FA-AAP strength, and the maximum aggregate size should not exceed 1/5 of the minimum spacing of the formwork, 1/3 of the thickness of the concrete slab, and 3/4 of the minimum spacing of reinforcement. Furthermore, the grading curves of aggregate in EN 206 are also suggested for the selection of aggregates.

3.3.2.3. Mix proportion calculation.
The quality of the aggregate phase has no direct influence on the compressive strength of BFS/FA-ACC when it has higher strength than BFS/FA-AAP. However, its content in concrete could greatly influence the cost and workability of BFS/FA-AAC. The design of aggregate content is mainly a balance between them.

The slump value and cohesion of BFS/FA-AAC, as the two most representative indicators of workability, are closely related to the content and characteristic of aggregates. Generally, the slump of BFS/FA-AAC increases with: 1) a larger maximum aggregate size (it is worth noting that the potential cracking problem caused by excess maximum aggregate size as in PC might no longer exist in BFS/FA-AAC due to a denser internal transition zone); 2) a higher content of larger size aggregate (within the suggested grading curves in EN 206); 3) a smoother surface of aggregate; 4) a higher paste/aggregate ratio (eg: water content within 160–195 kg/m^3 when the maximum aggregate size is 16 mm). The cohesion of BFS/FA-AAC increases with a higher fine/coarse aggregate ratio and a higher paste/aggregate ratio.

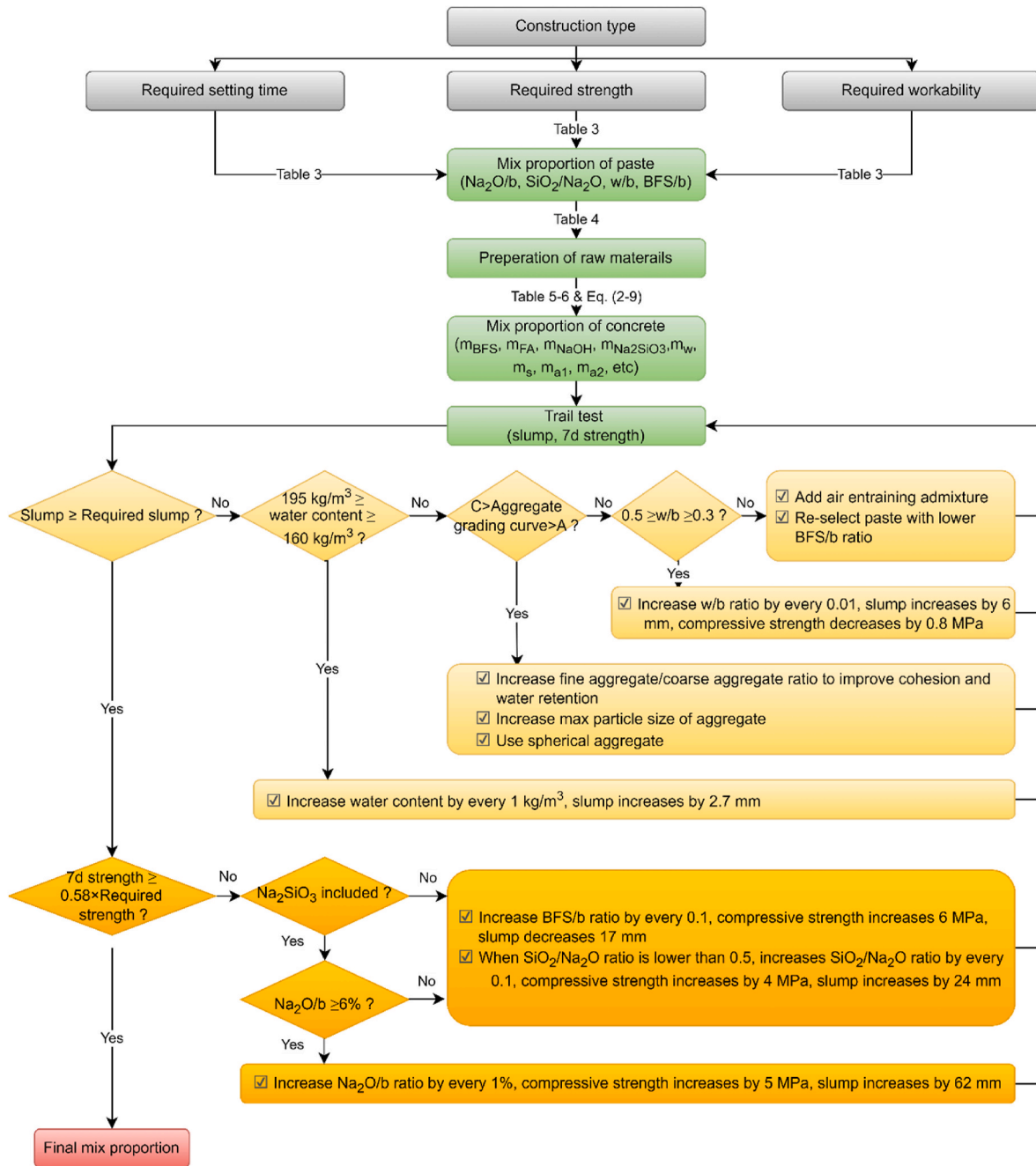However, it is not suggested to pursue high workability by over-

Fig. 10. Mix design procedure of BFS/FA-AAC.

raising the paste/aggregate ratio since the cost of BFS/FA-AAP is much higher than aggregate. Therefore, the principle of designing the aggregate phase of BFS/FA-AAC is to increase the aggregate content as much as possible without sacrificing the workability [60]. Previous researchers have found that the finer the sand, and the larger the maximum size of aggregate, the higher the volume of aggregate is allowed in 1 m³ concrete with still satisfied workability (see Table 5). With this concept, the maximum aggregate size could be designed by the dimension of structure and Table 4. After that, the dry bulk volume of coarse aggregate could be decided by the fineness modulus of the selected sand and Table 5.

After determining the mixture proportion of BFS/FA-AAP and the dry bulk volume of coarse aggregate, the mass of different components in 1 m³ of concrete could be designed by the closest packing theory, as shown in Fig. 11. After the largest size coarse aggregate fills the designed

dry bulk volume of 1 m³ concrete, assuming that each smaller size coarse aggregate fills the pores volume left by the previous filling, the mass of coarse aggregate could be calculated by Eqs. (2 and (3). Subsequently, the sand will fill the pores volume left by filling the smallest size of coarse aggregate to create the closest packing of aggregate in the 1 m³ concrete for the largest economical benefits. And the remaining volume in the 1 m³ concrete will be filled with BFS/FA-alkali activated mortar for adjusting the workability of the BFS/FA-AAC. The mass of sand could be calculated by Eq. (4). A sand/coarse aggregate ratio (β) is introduced for adjusting the workability of BFS/FA-AAC. The higher the β value (associated with the sand percentage in the BFS/FA-alkali activated mortar), the higher the cohesion and the lower slump that BFS/FA-AAC could achieve. Considering the grading curves principle of EN 206, the β value could be calculated by conversion, as suggested in Table 6. The mass of BFS, FA, NaOH, Na_2SiO_3, and water could be calculated by Eqs.

Table 3
BFS/FA-AAP table [29].

Mix design of AAP	AAP grade	BFS/b	2	4	6	8	10
			Na₂O/b (%) — SiO₂/Na₂O				
w/b=0.4 Note: with every 0.1 increase of w/b ratio, compressive strength decreases by 14 MPa, flowability increases by 47 mm	32.5	0			0.89-2.45 ☆	0.90-2.71 □◇☆	1.18-2.71 ◈○△□
		0.25	0.78-2 ▲▮	0.31-0.72 ▮◈○	0.20-0.52 ◉▲▮◈	0.27-0.56 ○△□	0.48-0.80 ●▲■◆
		0.5	0.35-0.69 ■◆★◉	0.04-0.26 ■◆★	0-0.16 ◆	0.05-0.23 ★◉▲	0.26-0.44 ●▲■
		0.75	0.16-0.38 ▲■◆	0-0.07 ■		0-0.07 ★	0.14-0.27 ▲■
		1	0.06-0.22 ●▲				0.06-0.17 ■
Setting time (min)	42.5	0.25		0.72-2.34 △□	0.52-0.96 ○△□◇	0.56-0.96 □◇	0.80-1.25 ★◉▲▮◈
Initial>45 Final<600		0.5	0.69-2.09 ◉	0.26-0.53 ◉▲▮	0.16-0.38 ◆★◉	0.23-0.44 ▮◈	0.44-0.66 ●▲
Initial>240 Final>600		0.75	0.38-0.65 ◆★	0.07-0.24 ■◆★	0-0.14 ■	0.07-0.21 ◉	0.27-0.42 ●▲
		1	0.22-0.40 ▲■	0-0.08 ▲		0-0.08 ◆	0.17-0.29 ▲
5 min flowability Note: flowability increase with SiO₂/Na₂O ratio	52.5	0.25			0.96-2 △○◇	0.96-3 △□◇	1.25-2.65 ◈○△
● 80-90 mm		0.5		0.53-0.90 ◆	0.38-0.64 ▲▮◈	0.44-0.68 ○△	0.66-0.92 ■◆★◉
▲ 90-100 mm		0.75	0.65-1.12 ★	0.24-0.44 ★◉▲	0.14-0.31 ◆★	0.21-0.37 ▲▮	0.42-0.59 ●
■ 100-110 mm		1	0.40-0.62 ◆	0.08-0.22 ▲■	0-0.13 ▲	0.08-0.20 ◆★	0.29-0.41 ●
◆ 110-120 mm	62.5	0.5		0.90-2.16 ○	0.64-0.99 ◈	0.68-0.99 △	0.92-1.28 ◉▲▮
★ 120-130 mm		0.75	1.12-1.66 ★◉	0.44-0.68 ▮□	0.31-0.49 ◉▲	0.37-0.54 ▮◈○	0.59-0.78 ●▲
◉ 130-140 mm		1	0.62-0.94 ◆	0.22-0.38 ◆★	0.13-0.26 ■	0.20-0.32 ◉	0.41-0.54 ●
▲ 140-150 mm	72.5	0.5			0.99-2.34 ○	0.99-1.55 △	1.28-2.61 ▮◈
▮ 150-160 mm		0.75		0.68-1.04 ◈	0.49-0.72 ▮◈	0.54-0.75 ○	0.78-1 ■◆★
◈ 160-170 mm		1	0.94-1.84 ◆★	0.38-0.57 ★◉	0.26-0.41 ◆★	0.32-0.46 ▲	0.54-0.69 ●
○ 170-180 mm	82.5	0.5				1.55-2.07 ○	
△ 180-190 mm		0.75		1.04-2.02 ◈○	0.72-1.01 ◈○△	0.75-1 ○△	1-1.30 ◉▲
□ 190-200 mm		1		0.57-0.80 ▲	0.41-0.57 ◉	0.46-0.62 ▮	0.69-0.86 ▲■
◇ 200-210 mm	92.5	0.75			1.01-2.32 △□	1-1.40 △□	1.30-2.59 ▲▮◈
☆ 210-240 mm		1		0.80-1.16 ▲▮	0.57-0.77 ▲	0.62-0.80 ◈	0.86-1.06 ◆
	>102.5	0.75				1.40-2.22 ○△□	
		1		1.16-1.90 ▮	0.77-2.57 ▮◈	0.80-2.82 ◈	1.06-2.84 ★◉▲

Table 4
Requirement of raw materials [32].

Material	Physical properties	Chemical properties
BFS	Optimal: 4000-5500 cm²/g; Glassy phase >90%	Basicity coefficient (kb) $\frac{CaO + MgO}{SiO_2 + Al_2O_3} \geq 1$; Quality coefficient (kq) $\frac{CaO + MgO + Al_2O_3}{SiO_2 + TiO_2} \geq 1.4$; $0.5 \leq \frac{CaO}{SiO_2} \leq 2$; $0.1 \leq \frac{Al_2O_3}{SiO_2} \leq 0.6$; $S \leq 2.5\%$; $TiO_2 \leq 4\%$
FA	80 %–90% particle ≤ 45 μm; Glassy phase >50%	Reactive $SiO_2 \geq 25\%$; Reactive $\frac{SiO_2}{Al_2O_3} \geq 1.5$; $Fe_2O_3 \leq 10\%$; $CaO \leq 10\%$; $SO_3 \leq 3\%$; $LOI \leq 5\%$; Free lime <1%; Free moisture <3%
Aggregate		Aggregate strength: should be larger than the required strength of BFS/FA-AAC; Aggregate grading: EN 206; Maximum aggregate size: should not exceed 1/5 of the minimum spacing of the formwork, 1/3 of the thickness of the concrete slab, and 3/4 of the minimum spacing of reinforcement.

Table 5
Dry bulk volume of coarse aggregate per unit volume of concrete (ACI 211.1–91).

Maximum size of aggregate		Dry bulk volume of rodded coarse aggregate per unit volume of concrete for fineness modulus of sand of:			
mm	in.	2.40	2.60	2.80	3.00
10	3/8	0.50	0.48	0.46	0.44
12.5	1/2	0.59	0.57	0.55	0.53
20	3/4	0.66	0.64	0.62	0.60
25	1	0.71	0.69	0.67	0.65
40	1 1/2	0.75	0.73	0.71	0.69
50	2	0.78	0.76	0.74	0.72
70	3	0.82	0.80	0.78	0.76
150	6	0.87	0.85	0.83	0.81

(5)–(9) according to the mixture proportion of BFS/FA-AAP. In which: m is the required mass of material in 1 m³ of concrete; ρ is the apparent particle density of aggregates, which could be obtained by aggregate characterization; v_b is the dry bulk volume of coarse aggregate per volume of concrete, which could be obtained from Table 5. v_c is the void ratio of aggregates, which could be obtained by aggregate characterization; C is the concentration of the equivalent (water, Na₂O, SiO₂) in sodium silicate activator; β is the sand/coarse aggregate ratio, which could be obtained by Table 6.
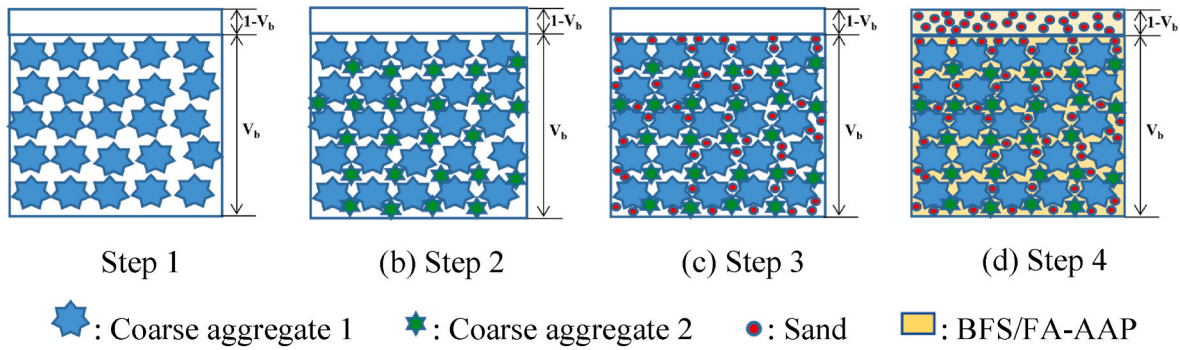
Step 1   (b) Step 2   (c) Step 3   (d) Step 4

✦ : Coarse aggregate 1   ✦ : Coarse aggregate 2   • : Sand   ▢ : BFS/FA-AAP

Fig. 11. The closest packing model of BFS/FA-AAC.

$$m_{a1} = \rho_{a1} \bullet (1 - v_{ca1}) \bullet v_b \tag{2}$$

$$m_{a2} = \rho_{a2} \bullet (1 - v_{ca2}) \bullet v_{ca1} \bullet v_b \tag{3}$$

$$m_s = \beta \bullet \rho_s \bullet v_b \bullet (1 - v_{ca1} \bullet v_{ca2}) \tag{4}$$

$$\frac{m_{BFS}}{m_{BFS} + m_{FA}} = \frac{BFS}{b} \tag{5}$$

$$\frac{m_{Na2SiO3} \bullet C_{SiO2}}{m_{BFS} + m_{FA}} = \frac{Na_2O}{b} \bullet \frac{SiO_2}{Na_2O} \tag{6}$$

$$\frac{0.775 m_{NaOH} + m_{Na2SiO3} \bullet C_{Na2O}}{m_{BFS} + m_{FA}} = \frac{Na_2O}{b} \tag{7}$$

$$\frac{0.225 m_{NaOH} + m_{Na2SiO3} \bullet C_w + m_w}{m_{BFS} + m_{FA}} = \frac{w}{b} \tag{8}$$

$$\frac{m_{a1}}{\rho_{a1}} + \frac{m_{a2}}{\rho_{a2}} + \frac{m_s}{\rho_s} + \frac{m_{BFS}}{\rho_{BFS}} + \frac{m_{FA}}{\rho_{FA}} + \frac{m_{NaOH}}{\rho_{NaOH}} + \frac{m_{Na2SiO3}}{\rho_{Na2SiO3}} + \frac{m_w}{\rho_w} = 1 \tag{9}$$

Table 6
The sand/coarse aggregate ratio (EN 206).

Maximum aggregate size (mm)	Sand/coarse aggregate ratio (v/v) for maximum sand size (mm) of:				
	1	2	3	4	5
8	0.27–1.33	0.43–2.45	0.92–3.55	1.56–5.67	2.23–7.33
16	0.14–0.96	0.27–1.63	0.41–2.15	0.56–2.85	0.67–3.35
32	0.09–0.72	0.16–1.13	0.22–1.44	0.30–1.86	0.79–4.00
63	0.06–0.64	0.12–0.96	0.18–1.13	0.23–1.44	0.52–2.70

3.3.2.4. Rules of thumb. To verify the performance of the preliminary designed mixture, a trial test should be carried out. Based on section 3.2, the predictive formula could evaluate the compressive strength of BFS/FA-AAC above 7 d with high accuracy. Therefore, the most representative and easily available characteristics: slump value and 7 d compressive value are considered performance indicators of BFS/FA-AAC. Only when they are tested to be higher than the required slump value and the required 7d strength (approximately 0.58 of the required 90 d compressive strength [29]), respectively, can the mixture be considered qualified.

Otherwise, the corresponding measurements should be taken to adjust the mixture proportion. Previous research has revealed that despite the differences in other ratios, not only the compressive strength but also the slump of BFS/FA-AAC shows a similar growth rate with the change of certain factors, as shown in Fig. 12. The data regarding the slump and compressive strength is obtained by the experiments of this paper and the previous research [29]. The rate of change of slump or compressive strength with each factor is derived by linear fitting. It is worth striking that the 7 d compressive strength is 0.58 multiplied by the 90 d rate of change value. According to these experimental results, a

"rule of thumb" is proposed to adjust the trial mixture proportion, as follows:

When the test slump value is lower than the required slump value, several rules could be adopted, as follows:

1) When the water content of BFS/FA-AAC is within 160–195 kg/m^3, with every 1 kg/m^3 increase (or decrease) of water in the mixture, the slump value could increase (or decrease) by 2.7 mm (see Fig. 12 (a and b)). The deviation is 0.9 mm.

2) When the Aggregate grading curve is below the C curve and above the A curve in EN 206, the slump of BFS/FA-AAC could be increased by increasing the maximum particle size of the aggregate or using the spherical aggregate. The cohesion and the water retention of BFS/FA-AAC could be improved by increasing the fine aggregate/coarse aggregate ratio.

3) When the w/b ratio is between 0.3 and 0.5, with every 0.01 increase (or decrease) of the w/b ratio, the slump of BFS/FA-AAC is expected to increase (or decrease) by 6 mm, and the compressive strength of BFS/FA-AAC is supposed to decrease (or increase) by 0.8 MPa (see Fig. 12(c and d)). The deviation of the slump and compressive strength is 5 mm and 0.29 MPa, respectively.

4) Except for the measurements above, the slump of BFS/FA-AAC could be improved as well by adding air-entraining admixture or re-select a mixture from Table 3 with a lower BFS/b ratio.

Likewise, if the required 7 d compressive strength is not achieved, the adjustment of the mixture could be conducted according to the compressive strength prediction as follows:

1) When sodium silicate is included in the mixture and the Na$_2$O/b ratio is lower than 6%, with every 1% increase (or decrease) of the Na$_2$O/b

(a) 5 min slump

(b) 90 d compressive strength

(c) 5 min slump

(d) 90 d compressive strength

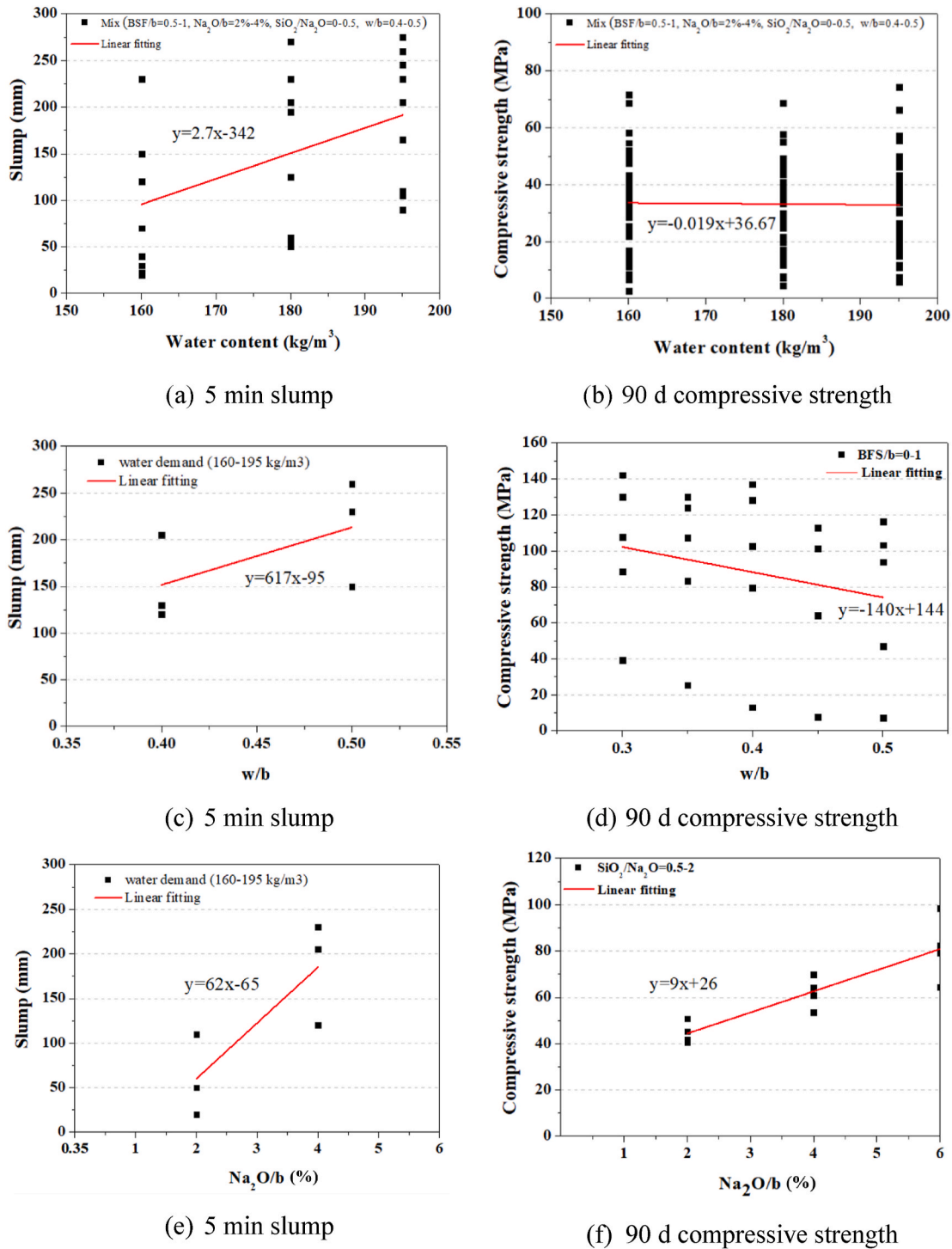(e) 5 min slump

(f) 90 d compressive strength

Fig. 12. Rules of thumb.

ratio, the compressive strength of BFS/FA-AAC could increase (or decrease) by 5 MPa, and the slump could increase (or decrease) by 62 mm (see Fig. 12(e and f)). The deviation of the slump and compressive strength is 14 mm and 1.79 MPa, respectively.

2) When sodium silicate is not included, or the Na_2O/b ratio is higher than 6%, with every 0.1 increase (or decrease) of the BFS/b ratio, the compressive strength of BFS/FA-AAC could increase (or decrease) by 6 MPa, while the slump could decrease (or increase) by 17 mm (see Fig. 12(g and h)). The deviation of the slump and compressive strength is 8 mm and 0.47 MPa, respectively. Besides, if the SiO_2/

Na_2O ratio is lower than 0.5, with every 0.1 increase (or decrease) of the SiO_2/Na_2O ratio, the compressive strength of BFS/FA-AAC could increase (or decrease) by 4 MPa, and the slump could increase (or decrease) by 24 mm (see Fig. 12(i and j)). The deviation of the slump and compressive strength is 6 mm and 1.79 MPa, respectively.
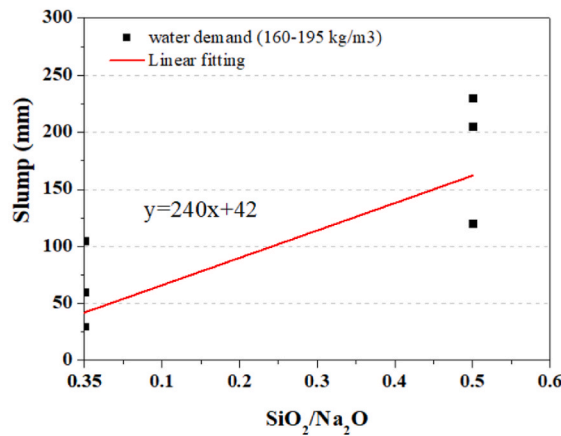
3.3.3. A mix design case

A mix design case was conducted to illustrate the proposed mix design method above. Assuming that the columns of a building that are exposed to a normal environment (no durability problems) would be
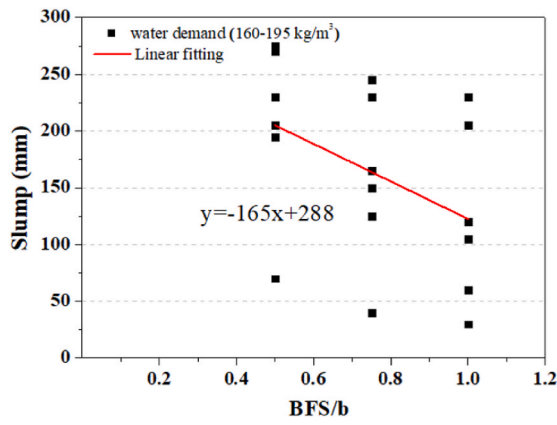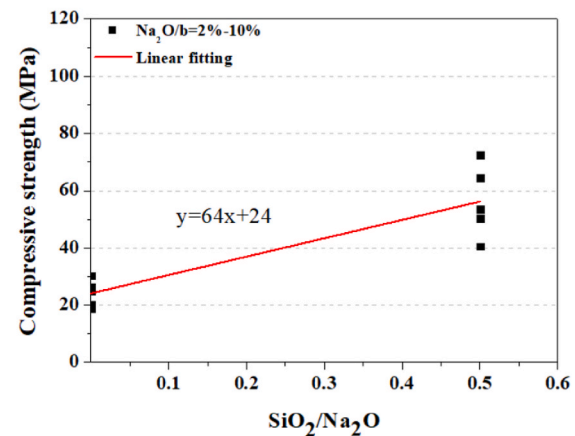
(g) 5 min slump
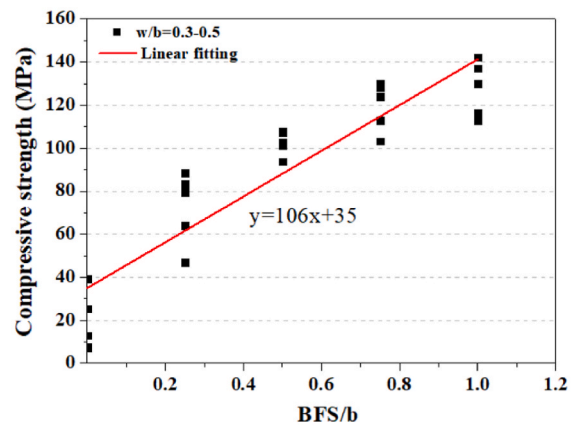
(h) 90 d compressive strength

(i) 5 min slump

(j) 90 d compressive strength

Fig. 12. (*continued*).

made of BFS/FA-AAC. The size of the column sections and the spacing of the reinforcement require a slump of class S3 (100–150 mm) and a maximum aggregate size of 16 mm. The compressive strength at maturity (90 d) requirement is C 40. The BFS/FA-AAC could be designed by the following steps:

Step 1: According to the compressive strength requirement, slump requirement, and construction type (setting time meets normal construction requirements), the mix proportion of BFS/FA-AAP could be designed by Table 3. The trial mix proportion of BFS/FA-AAP could be: BFS/b ratio of 0.75, Na$_2$O/b ratio of 4%, SiO$_2$/Na$_2$O ratio of 0.34, w/b ratio of 0.42 (see the detailed design process in the previous research) [29].

Step 2: According to the construction type and the availability of the raw materials, the BFS, FA, sodium hydroxide, sodium silicate, sand, and coarse aggregate could be prepared following the requirements of Table 4. In this case study, the characteristic of the selected raw materials is depicted in Section 2.1.

Step 3: According to the closest packing theory (most economy), the mass of different components (BFS, FA, NaOH, Na$_2$SiO$_3$, additional water, aggregate 1, aggregate 2, sand) in BFS/FA-AAC could be calculated according to Table 5, Table 6, and Eqs. (2)–(9). The dry bulk volume of coarse aggregate per unit volume of concrete is 0.57, obtained by linear interpolation. The sand/coarse aggregate ratio could be 0.56, which is the lowest value when the maximum sand size and the maximum aggregate size are 4 mm and 16 mm, respectively. This is for obtaining a preferable slump value

considering the required high slump class (S3). The detailed calculation process is presented as follows:

$$m_{a1} = 1548 \times 0.57 = 882.360 \text{ kg}$$

$$m_{a2} = 1559 \times 0.57 \times \left(1 - \frac{1548}{2619}\right) = 363.392 \text{ kg}$$

$$m_s = 0.56 \times 2644 \times \left(\frac{882.360}{2619} + \frac{363.392}{2589}\right) = 706.661 \text{ kg}$$

$$m_{BFS} = 237.786 \text{ kg}$$

$$m_{FA} = 79.262 \text{ kg}$$

$$m_{NaOH} = 14.843 \text{ kg}$$

$$m_{Na2SiO3} = 15.679 \text{ kg}$$

$$m_w = 119.780 \text{ kg}$$

Step 4: According to the experimental (the first trial test) results, the slump value is 0 mm (too dry). Based on Fig. 10, higher water content is required for obtaining better workability. By increasing the water content to 160 kg/m^3, the mixture proportion could be adjusted as follows:

$$m_{BFS} = \frac{160}{0.42} \times 0.75 = 285.714 \text{ kg}$$

$$m_{FA} = \frac{160}{0.42} \times (1 - 0.75) = 95.238 \text{ kg}$$

$$m_{Na2SiO3} = \frac{\frac{160}{0.42} \times 0.04 \times 0.34}{0.275} = 18.840 \text{ kg}$$

$$m_{NaOH} = \left(0.04 \times \frac{160}{0.42} - 18.840 \times 0.0825\right) \times \frac{80}{62} \times \frac{1}{0.99} = 17.835 \text{ kg}$$

$$m_w = 160 - 18.840 \times 0.6425 - \frac{17.835 \times 0.99 \times 18}{80} = 143.923 \text{ kg}$$

required compressive strength is 23 MPa), respectively, and both meet the requirements. As a result, the determined mixture proportion of BFS/FA-AAC is presented in Table 7.

The case study not only demonstrates the feasibility of the BFS/FA-AAC mix design method, but also proves the accuracy of the compressive strength prediction method [29], and the environmental values of using BFS/FA-AAC. The comparison between the tested compressive strength and the PF-predicted compressive strength is presented in Fig. 13. The error between them is approximately 2 MPa, which further validates the accuracy of the PF model (prediction intervals: the Na_2O/b ratio of 0 %–10%, the SiO_2/Na_2O ratio of 0–2, the w/b ratio of 0.3–0.5, the BFS/b ratio of 0–1, and sealed curing at ambient temperature, the prediction interval of the compressive strength is 95%.). Besides, the economic and environmental values of BFS/FA-AAC and PC concrete with similar performance were compared (see Table 7). The cost and the

$$m_s = \left(1 - \frac{285.714}{2890} - \frac{95.238}{2300} - \frac{18.840}{1350} - \frac{17.835}{2130} - \frac{143.923}{997}\right) \times \frac{0.56}{1 + 0.56} \times 2644 = 657.788 \text{ kg}$$

$$m_{a1} = \left(1 - \frac{285.714}{2890} - \frac{95.238}{2300} - \frac{18.840}{1350} - \frac{17.835}{2130} - \frac{143.923}{997} - \frac{657.788}{2644}\right) \times \frac{2619}{1 + \frac{(2619-1548)\times 1559}{1548 \times 2589}} = 821.336 \text{ kg}$$

$$m_{a2} = \left(\frac{1}{1548} - \frac{1}{2619}\right) \times 821.336 \times 1559 = 338.260 \text{ kg}$$

Step 5: According to the experiments (the second trial test) results, the slump and 7 d compressive strength of the designed BFS/FA-AAC are 115 mm (the required slump is 100–150 mm) and 31 MPa (the

global warming potential (GWP) per unit volume of concrete were calculated by the raw materials price and GWP value collected from the literature. The cost of 1 cubic meter of the mixture is the sum of the prices of each raw material. And the GWP value of 1 cubic meter of the mixture is the sum of the GWP of each raw material. GWP of a chemical substance is defined as the ratio of the time integral of the radiation effect over a period of time from the start of the release of 1 kg of the substance to the time integral of the release of 1 kg of reference gas (CO_2) under the same conditions. The results show that the cost and GWP of 1 cubic meter of the case study BFS/FA-AAC mixture are 79 EUR and 60 kg CO_2 eq, respectively. Although the price of the case study BFS/FA-AAC mix is similar to that of PC concrete, its GWP is 82% lower than that of PC concrete. It indicates that the utilization of BFS/FA-AAC proposed in the case study has promising environmental benefits.

Table 7
Final mix proportion and its economical and environmental value compared to PC concrete.

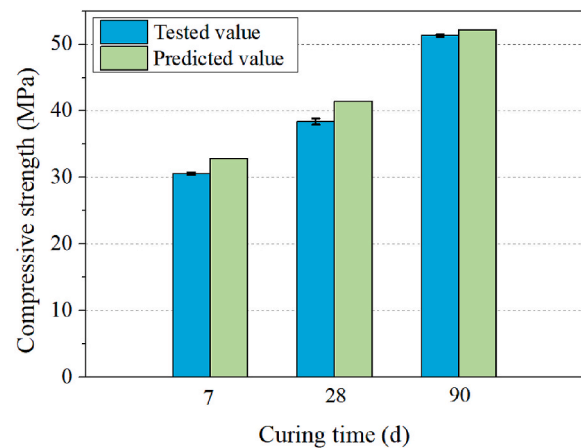|	Price (EUR/kg)	GWP (kg CO_2 eq)	Ref. mix [61] (kg/m³)	Case-mix (kg/m³)
Cement I	0.093 [62]	8.44×10^{-1} [63]	391	0
BFS	0.077 [64]	1.69×10^{-2} [63]	0	286
FA	0.035 [64]	5.26×10^{-3} [63]	0	95
NaOH pearls	0.354 [62]	1.6 [65]	0	18
Na_2SiO_3 solution	0.79 [62, 64]	1.14 [63]	0	19
Water	0.001 [62]	1.55×10^{-4} [63]	181	144
Superplasticizer	0.274 [66]	7.49×10^{-1} [63]	0.782	0
Air entraining admixture	1.58 [67]	7.49×10^{-1} [63]	0.782	0
Sand	0.009 [62]	2.4×10^{-3} [63]	572	658
Aggregate 8–16 mm	0.023 [62]	2.4×10^{-3} [63]	635	821
Aggregate 2–8 mm	0.023 [62]	1.55×10^{-3} [63]	795	338
Slump (mm)	N/A	N/A	110	115
Compressive strength at maturity (MPa)	N/A	N/A	49.5	51.3
Cost (EUR/m³)	N/A	N/A	76	79
GWP (kg CO_2 eq/m³)	N/A	N/A	335	60

Fig. 13. Comparison between tested and predicted compressive strength of the case.

4. Conclusions

In this paper, the control factors and their effect on the slump and compressive strength of BFS/FA-AAC were investigated. A practical mix design method for BFS/FA-AAC serving in ordinary environments was proposed and a case study was carried out to further validate the mix design method. Accordingly to the research, the main conclusion could be extracted as follow:

(1) Unlike the design of PC concrete, the mixture composition of the paste should be highly concerned in the slump design of BFS/FA-AAC. The slump of BFS/FA-AAC might be influenced by water content, maximum aggregate size, aggregate grading, and the mixture composition of the paste (the Na_2O/b ratio, the SiO_2/Na_2O ratio, the BFS/b ratio, and the w/b ratio).

(2) The water content (within 160–195 kg/m^3) are found to have little influence on the compressive strength of BFS/FA-AAC. A wider range of water content is suggested to be investigated in the future study to further explore the boundaries of the paste content in BFS/FA-AAC that ensure stable performance (without affectable segregation, shrinkage, insufficient aggregate bonding, and harmful pores introduction problems caused by too large or too small paste/aggregate ratio).

(3) Within the water content of this study, the compressive strength of BFS/FA-AAC is determined by the control factors, including the Na_2O/b ratio, the SiO_2/Na_2O ratio, the BFS/b ratio, the w/b ratio, and the curing time.

(4) A straightforward mix design calculation method of BFS/FA-AAC serving in ordinary environments is established. Besides, a series of measurements considering slump and compressive strength are proposed for further adjusting the BFS/FA-AAC mixture in the trial test.

(5) The BFS/FA-AAC mixture designed by the mix design method not only meets the expected fresh and hardened properties but also has high environmental benefits.

(6) The mechanical predictive method of BFS/FA-AAC shows high accuracy. The difference between the predicted compressive strength in the case study and the tested compressive strength is about 2 MPa.

(7) In future research, the proposed mix design method could be improved by investigating the effect of control factors on the durability and sustainability of BFS/FA-AAC, so as to develop regulations regarding long-term performance. The influence of chemical composition, particle size distribution, and glassy content of precursors on the performance of BFS/FA-AAM is suggested for systematic investigation, and a modified predictive method is expected to be proposed.

Declaration of competing interest

The authors declare that they have no known competing financial interests or personal relationships that could have appeared to influence the work reported in this paper.

Data availability

Data will be made available on request.

Acknowledgments

References

[1] G. Habert, J. De Lacaillerie, Roussel, An environmental evaluation of geopolymer based concrete production: reviewing current research trends, J. Clean. Prod. 19 (11) (2011) 1229–1238.

[2] L.K. Turner, F.G. Collins, Carbon dioxide equivalent (CO2-e) emissions: a comparison between geopolymer and OPC cement concrete, Construct. Build. Mater. 43 (2013) 125–130.

[3] J.S. van Deventer, J.L. Provis, P. Duxson, D.G. Brice, Chemical research and climate change as drivers in the commercial adoption of alkali activated materials, Waste Biomass Valorization 1 (1) (2010) 145–155.

[4] J. Davidovits, Geopolymer cements to minimize carbon dioxide greenhouse warming, Ceram. Trans. 37 (1) (1993) 165–182.

[5] F. Preston, J. Lehne, Making Concrete Change Innovation in Low-Carbon Cement and Concrete, 2018.

[6] K. Arbi, M. Nedeljkovic, Y. Zuo, S. Grünewald, A. Keulen, G. Ye, Experimental study on workability of alkali activated fly ash and slag-based geopolymer concretes, in: Geopolymers: the Route to Eliminate Waste Emissions in Ceramic Cement Manufacturing, 2015, pp. 75–78.

[7] M. Nedeljkovic, K. Arbi, Y. Zuo, G. Ye, Physical properties and pore solution analysis of alkali activated fly ash-slag pastes, in: Proceedings of the International RILEM Conference on Materials, Systems and Structures in Civil Engineering, Conference Segment on Concrete with Supplementary Cementitious Materials, Lyngby, Denmark, 2016, pp. 22–24.

[8] M. Nedeljković, Y. Zuo, K. Arbi, G. Ye, Carbonation resistance of alkali-activated slag under natural and accelerated conditions, J.Sustain.Metall. 4 (1) (2018) 33–49.

[9] M. Nedeljković, Y. Zuo, K. Arbi, G. Ye, Natural Carbonation of Alkali-Activated Fly Ash and Slag Pastes, High Tech Concrete, Where Technology and Engineering Meet, Springer, 2018, pp. 2213–2223.

[10] Z. Tan, G. De Schutter, G. Ye, Y. Gao, L. Machiels, Influence of particle size on the early hydration of slag particle activated by Ca (OH) 2 solution, Construct. Build. Mater. 52 (2014) 488–493.

[11] Y. Ma, J. Hu, G. Ye, The effect of activating solution on the mechanical strength, reaction rate, mineralogy, and microstructure of alkali-activated fly ash, J. Mater. Sci. 47 (11) (2012) 4568–4578.

[12] A.M. Fernandez-Jimenez, A. Palomo, C. Lopez-Hombrados, Engineering properties of alkali-activated fly ash concrete, ACI Mater. J. 103 (2) (2006) 106.

[13] M. Sofi, J. Van Deventer, P. Mendis, G. Lukey, Engineering properties of inorganic polymer concretes (IPCs), Cement Concr. Res. 37 (2) (2007) 251–257.

[14] A. Rashad, A comprehensive overview about the influence of different additives on the properties of alkali-activated slag–A guide for Civil Engineer, Construct. Build. Mater. 47 (2013) 29–55.

[15] M.O. Yusuf, M.A.M. Johari, Z.A. Ahmad, M.J.M. Maslehuddin, Evolution of alkaline activated ground blast furnace slag–ultrafine palm oil fuel ash based concrete, Mater. Des. 55 (2014) 387–393.

[16] M.O. Yusuf, M.A.M. Johari, Z.A. Ahmad, M.J.M. Maslehuddin, Design, Effects of H2O/Na2O molar ratio on the strength of alkaline activated ground blast furnace slag-ultrafine palm oil fuel ash based concrete, Mater. Des 56 (2014) 158–164.

[17] R. Anuradha, V. Sreevidya, R. Venkatasubramani, B.V. Rangan, Modified guidelines for geopolymer concrete mix design using Indian standard, Asian.J. Civ. Eng. 13 (2012) 353–364.

[18] M.S. Reddy, P. Dinakar, B.H. Rao, Mix design development of fly ash and ground granulated blast furnace slag based geopolymer concrete, J. Build. Eng. 20 (2018) 712–722.

[19] A. Rafeet, R. Vinai, M. Soutsos, W. Sha, Guidelines for mix proportioning of fly ash/GGBS based alkali activated concretes, Construct. Build. Mater. 147 (2017) 130–142.

[20] M.T. Junaid, O. Kayali, A. Khennane, J. Black, A mix design procedure for low calcium alkali activated fly ash-based concretes, Construct. Build. Mater. 79 (2015) 301–310.

[21] M.N. Hadi, N.A. Farhan, M.N. Sheikh, Design of geopolymer concrete with GGBFS at ambient curing condition using Taguchi method, Construct. Build. Mater. 140 (2017) 424–431.

[22] R.R. Bellum, R. Nerella, S.R.C. Madduru, C. Indukuri, Mix design and mechanical properties of fly ash and GGBFS-synthesized alkali-activated concrete (AAC), Infrastructure 4 (2) (2019) 20.

[23] M.N. Hadi, H. Zhang, S. Parkinson, Optimum mix design of geopolymer pastes and concretes cured in ambient condition based on compressive strength, setting time and workability, J. Build. Eng. 23 (2019) 301–313.

[24] P.S. Deb, P. Nath, P.K. Sarker, The effects of ground granulated blast-furnace slag blending with fly ash and activator content on the workability and strength properties of geopolymer concrete cured at ambient temperature, Mater. Des. 62 (2014) 32–39, 1980-2015.

[25] G. Mounika, B. Ramesh, J.S. Kalyana Rama, Experimental investigation on physical and mechanical properties of alkali activated concrete using industrial and agro waste, Mater. Today: Proc. 33 (2020) 4372–4376.

[26] A. Kar, Characterizations of Concretes with Alkali-Activated Binder and Correlating Their Properties from Micro-to Specimen Level, Ph.D. thesis, West Virginia University, 2013.

[27] R. Gopalakrishnan, K. Chinnaraju, Durability of ambient cured alumina silicate concrete based on slag/fly ash blends against sulfate environment, Construct. Build. Mater. 204 (2019) 70–83.

[28] M. Nedeljkovic, Z. Li, G. Ye, Setting, strength, and autogenous shrinkage of alkali-activated fly ash and slag pastes: effect of slag content, Materials 11 (11) (2018).

[29] B. Sun, Y. Sun, G. Ye, G. De Schutter, A mix design methodology of slag and fly ash-based alkali-activated paste, Cement Concr. Compos. 126 (2022).

[30] T. Phoo-ngernkham, C. Phiangphimai, N. Damrongwiriyanupap, S. Hanjitsuwan, J. Thumrongvut, P. Chindaprasirt, A mix design procedure for alkali-activated high-calcium fly ash concrete cured at ambient temperature, Adv. Mater. Sci. Eng. 2018 (2018) 1–13.

[31] N. Li, C. Shi, Z. Zhang, D. Zhu, H.J. Hwang, Y. Zhu, T. Sun, A mixture proportioning method for the development of performance-based alkali-activated slag-based concrete, Cement Concr. Compos. 93 (2018) 163–174.

[32] B. Sun, G. Ye, G. De Schutter, A review: reaction mechanism and strength of slag and fly ash-based alkali-activated materials, Construct. Build. Mater. 326 (2022), 126843.

[33] C.C. Hung, J. Chang, The influence of mixture variables for the alkali-activated slag concrete on the properties of concrete, J. Mar. Sci. Technol. 21 (3) (2013) 1.

[34] S. Haruna, B.S. Mohammed, M. Wahab, M. Liew, Effect of paste aggregate ratio and curing methods on the performance of one-part alkali-activated concrete, Construct. Build. Mater. 261 (2020) 120024.

[35] R. Vinai, A. Rafeet, M. Soutsos, W. Sha, The role of water content and paste proportion on physico-mechanical properties of alkali activated fly ash–ggbs concrete, J.Sustain.Metall. 2 (1) (2016) 51–61.

[36] E.P. Koehler, D.W. Fowler, C.F. Ferraris, S. Amziane, A new, portable rheometer for fresh self-consolidating concrete, ACI Mater. J. 233 (2005) 97.

[37] P.K. Mehta, P.J. Monteiro, Concrete: Microstructure, Properties, and Materials, McGraw-Hill Education, 2014.

[38] A. Allahverdi, E.N. Kani, S. Esmaeilpoor, Engineering, Effects of silica modulus and alkali concentration on activation of blast-furnace slag, Iran.J.Mater 5 (2) (2008) 32–35.

[39] H. Taghvayi, K. Behfarnia, M. Khalili, The effect of alkali concentration and sodium silicate modulus on the properties of alkali-activated slag concrete, J. Adv. Concr. 16 (7) (2018) 293–305.

[40] Z. Jiao, Y. Wang, W. Zheng, W. Huang, Engineering, Effect of dosage of alkaline activator on the properties of alkali-activated slag pastes, Adv. Mater. Sci. (2018) 2018.

[41] X. Gao, Q.L. Yu, H.J.H. Brouwers, Reaction kinetics, gel character and strength of ambient temperature cured alkali activated slag–fly ash blends, Construct. Build. Mater. 80 (2015) 105–115.

[42] C. Shi, D. Roy, P. Krivenko, Alkali-activated Cements and Concretes, CRC press, 2003.

[43] T.C. Powers, Structure and physical properties of hardened Portland cement paste, J. Am. Ceram. Soc. 41 (1) (1958) 1–6.

[44] G. Fang, Q. Wang, M. Zhang, Micromechanical analysis of interfacial transition zone in alkali-activated fly ash-slag concrete, Cement Concr. Compos. 119 (2021), 103990.

[45] G. Fang, M. Zhang, The evolution of interfacial transition zone in alkali-activated fly ash-slag concrete, Cement Concr. Res. 129 (2020), 105963.

[46] Z. Luo, W. Li, K. Wang, A. Castel, S.P. Shah, Comparison on the properties of ITZs in fly ash-based geopolymer and Portland cement concretes with equivalent flowability, Cement Concr. Res. 143 (2021) 106392.

[47] W. Lee, J. Van Deventer, The interface between natural siliceous aggregates and geopolymers, Cement Concr. Res. 34 (2) (2004) 195–206.

[48] A. Brough, A. Atkinson, Automated identification of the aggregate–paste interfacial transition zone in mortars of silica sand with Portland or alkali-activated slag cement paste, Cement Concr. Res. 30 (6) (2000) 849–854.

[49] R. San Nicolas, J.L. Provis, The interfacial transition zone in alkali-activated slag mortars, Frontiers in materials 2 (2015) 70.

[50] R. San Nicolas, S.A. Bernal, R.M. de Gutiérrez, J.S. van Deventer, J.L. Provis, Distinctive microstructural features of aged sodium silicate-activated slag concretes, Cement Concr. Res. 65 (2014) 41–51.

[51] V. Glukhovsky, Ancient, modern and future concretes, in: Proceedings of the First International Conference on Alkaline Cements and Concretes, Kiev, Ukraine, 1994, pp. 1–9.

[52] A. Palomo, P. Krivenko, I. Garcia-Lodeiro, E. Kavalerova, O. Maltseva, A. Fernández-Jiménez, A review on alkaline activation: new analytical perspectives, Mater. Construcción 64 (315) (2014).

[53] J. Li, Q. Yu, H. Huang, S. Yin, Difference in the reaction process of slag activated by waterglass solution and NaOH solution, Struct. Concr. 20 (5) (2019) 1528–1540.

[54] Y. Zuo, Experimental Study and Numerical Simulation of the Reaction Process and Microstructure Formation of Alkali-Activated Materials, Delft University of Technology, 2019.

[55] X. Ouyang, Y. Ma, Z. Liu, J. Liang, G. Ye, Effect of the sodium silicate modulus and slag content on fresh and hardened properties of alkali-activated fly ash/slag, Minerals 10 (1) (2020) 15.

[56] A. Rafeet, R. Vinai, M. Soutsos, W. Sha, Effects of slag substitution on physical and mechanical properties of fly ash-based alkali activated binders (AABs), Cement Concr. Res. 122 (2019) 118–135.

[57] A. Fernández-Jiménez, F. Puertas, I. Sobrados, J. Sanz, Structure of calcium silicate hydrates formed in alkaline-activated slag: influence of the type of alkaline activator, J. Am. Ceram. Soc. 86 (8) (2003) 1389–1394.

[58] G. Fang, W.K. Ho, W. Tu, M. Zhang, Workability and mechanical properties of alkali-activated fly ash-slag concrete cured at ambient temperature, Construct. Build. Mater. 172 (2018) 476–487.

[59] P. Nath, P.K.J.C. Sarker, Effect of GGBFS on setting, workability and early strength properties of fly ash geopolymer concrete cured in ambient condition, Construct. Build. Mater. 66 (2014) 163–171.

[60] F. De Larrard, Concrete Mixture Proportioning: a Scientific Approach, CRC Press, 1999.

[61] A. Nowak-Michta, Impact analysis of air-entraining and superplasticizing admixtures on concrete compressive strength, Procedia Struct. Integr. 23 (2019) 77–82.

[62] K. Shwekat, H.-C. Wu, Benefit-cost analysis model of using class F fly ash-based green cement in masonry units, J. Clean. Prod. 198 (2018) 443–451.

[63] C. Ouellet-Plamondon, G. Habert, Life Cycle Assessment (LCA) of Alkali-Activated Cements and Concretes, Handbook of Alkali-Activated Cements, Mortars and Concretes, Elsevier, 2015, pp. 663–686.

[64] L. Hoekstra, Most Efficient Use of Blast Furnace Slag and Fly Ash in Concrete, 2020, indiamart, 2022. Retrieved from, https://www.indiamart.com/proddetail/powder-sodium-carbonate-21182283488.html.

[65] R.A. Robayo-Salazar, J.M. Mejía-Arcila, R.M. de Gutiérrez, Eco-efficient alkali-activated cement based on red clay brick wastes suitable for the manufacturing of building materials, J. Clean. Prod. 166 (2017) 242–252.

[66] R.A. Robayo-Salazar, J.M. Mejía-Arcila, R.M. de Gutiérrez, Eco-efficient alkali-activated cement based on red clay brick wastes suitable for the manufacturing of building materials, J. Clean. Prod. 166 (2017) 242–252.

[67] I. Justo-Reinoso, B.J. Reeksting, C. Hamley-Bennett, A. Heath, S. Gebhard, K. Paine, Air-entraining admixtures as a protection method for bacterial spores in self-healing cementitious composites: healing evaluation of early and later-age cracks, Construct. Build. Mater. 327 (2022), 126877.